Received: 23 October 2016 | Revised: 7 January 2017 | Accepted: 9 January 2017
DOI: 10.1002/gj.2910

WILEY

RESEARCH ARTICLE

Petrogenesis and tectonic setting of the Middle Permian A-type granites in Altay, northwestern China: Evidences from geochronological, geochemical, and Hf isotopic studies

Yunlong Liu[1,2] | Hui Zhang[1] | Yong Tang[1] | Xin Zhang[1,2] | Zhenghang Lv[1] | Jingyu Zhao[1,2]

[1] Key Laboratory of High-temperature and High-pressure Study of the Earth's Interior, Institute of Geochemistry, Chinese Academy of Sciences, Guiyang, China

[2] University of Chinese Academy of Sciences, Beijing, China

Correspondence
Hui Zhang, Key Laboratory of High-temperature and High-pressure Study of the Earth's Interior, Institute of Geochemistry, Chinese Academy of Sciences, Guiyang 550081, China.
Email: zhanghui@mail.gyig.ac.cn

Funding information
National Natural Science Foundation of China, Grant/Award Number: 41372104; National Science Foundation of China, Grant/Award Number: 41073051

Handling editor: M. Santosh

The Jiangjunshan and Dakalasu alkali-feldspar granites are located in the central part of the Chinese Altay orogen. In this paper, we present detailed geochemical, zircon U–Pb, and Hf isotopic data of these granites. The Jiangjunshan and Dakalasu alkali-feldspar granites show a high content of SiO_2 (72.05–73.27 and 69.55–71.04 wt%, respectively), total alkalis ($Na_2O + K_2O$ = 8.41–8.71 and 7.24–8.66 wt%, respectively), and high-field strength elements (Zr + Nb + Ce + Y = 400.3–482.9 and 156.7–339.3 ppm, respectively), as well as high Ga/Al ratios (10,000 × Ga/Al = 3.46–4.19 and 2.62–3.28, respectively) and depletion in Ba, Nb, Sr, and Ti, showing geochemical characteristics similar to those of A-type granites. Zircon U–Pb dating of the Jiangjunshan and Dakalasu alkali-feldspar granites yielded weighted mean dating $^{206}Pb/^{238}U$ ages of 268.3 ± 1.9 and 270.4 ± 1.9 Ma, respectively, indicating that these granites intruded during the Permian. The Jiangjunshan and Dakalasu alkali-feldspar granites show highly variable zircon $\varepsilon_{Hf}(t)$ values ranging from −7.0 to +5.6, implying that these granites originated from a mixing of mantle-derived magma with crustal materials. Our data on the Jiangjunshan and Dakalasu alkali-feldspar granites, coupled with previous studies of Permian magmatism and metamorphism, suggest that the tectonic regime was in a postcollisional extensional environment in the Chinese Altay orogen during the Permian. Therefore, the change in stress from compression to extension and asthenospheric upwelling triggered by slab break-off plays a significant role in the generation of Jiangjunshan and Dakalasu alkali-feldspar granites.

KEYWORDS
Altay, A-type granite, Hf isotope, petrogenesis, tectonic setting, U–Pb dating, Xinjiang

1 | INTRODUCTION

The Central Asian Orogenic Belt is one of the largest and longest-lived accretionary orogenic belts on Earth, representing a typical region of massive continental crust growth (Jahn, 2004; Jahn, Wu, & Chen, 2000a; Jahn, Wu, & Chen, 2000b; Sengör & Natal'in, 1996; Sengör, Natal'in, & Burtman, 1993; Windley, Alexeiev, Xiao, Kröner, & Badarch, 2007). During its evolutionary history, numerous allochthonous materials, such as island arcs, seamounts, subduction–accretion complexes, ophiolites, and microcontinents, have been incorporated (Khain et al., 2002; Kovalenko et al., 2004; Kröner et al., 2011; Kröner et al., 2014; Wilhem, Windley, & Stampfli, 2012; Windley et al., 2002; Windley et al., 2007; Xiao & Santosh, 2014; Xiao et al., 2004; Zhang et al., 2015). The Chinese Altay is situated along the southwest margin of the Mongolian collage system and is juxtaposed with the Kazakhstan collage system to the south. Because of this key tectonic position, the Chinese Altay is considered an important region for studying the convergent processes and amalgamation between the Mongolian and Kazakhstan collage systems. Previous investigations have confirmed that the Chinese Altay constitutes a subduction–accretion complex built on the margin of Mongolian collage systems in the Early Paleozoic (Cai, Sun, Yuan, Zhao, Xiao, Long, & Wu, 2011b; Cai et al., 2014; Long et al., 2007; Long et al., 2010; Sun et al., 2008; Xiao et al., 2008; Xiao et al., 2009). However, there is much debate about its tectonic scenario in the Carboniferous to Permian, which is a critical period for its final amalgamation. Several models have been proposed for the Late Paleozoic tectonic evolution of the Chinese Altay, including oceanic subduction (Chen et al., 2006; Wan, Xiao, Windley, & Yuan, 2013; Xiao et al., 2011; Zhang et al., 2015), postcollisional extension (Gao & Zhou, 2013; Han, Ji, Song, Chen, &

Li, 2004; Su et al., 2011; Tong, Wang, Jahn, Sun, Hong, & Gao, 2014b; Tong, Wang, Siebel, Hong, & Sun, 2012; Zhang, Zhou, Kusky, Yan, Chen, & Zhao, 2009b), slab break-off (Gao & Zhou, 2013; Li, Zhang, Fu, Qian, Hu, & Ripley, 2012a), and mantle plume (Pirajno, Mao, Zhang, Zhang, & Chai, 2008; Tong, Xu, Cawood, Zhou, Chen, & Liu, 2014a; Zhang, Zou, Yao, & Dong, 2014a). Therefore, more systematic research is needed to unravel the tectonomagmatic events that have determined the tectonic evolution of the region.

Recently, we identified two A_2-type granites on the southern part of the Chinese Altay orogen. A-type granites were first catalogued by Loiselle and Wones (1979) and have been extensively studied due to their unusual origins and tectonic settings (Bonin, 2007; Collins, Beams, White, & Chappell, 1982; Creaser, Price, & Wormald, 1991; Dall'Agnol & de Oliveira, 2007; Eby, 1992; Frost & Frost, 1997; King, White, Chappell, & Allen, 1997; Whalen, Currie, & Chappell, 1987). Eby (1992) subdivided A-type granites into two subtypes and suggested that they may have different origins and tectonic settings. The A_1-type granites represent differentiates of magmas derived from ocean-island basalt (OIB)-like sources but emplaced in continental rifts or during intraplate magmatism. The A_2-type granites are derived from partial melting of continental crust or underplated mafic crust that has been through a cycle of continent-to-continent collision or a subduction zone; these granites originate in a postcollisional extensional setting.

In this paper, we present zircon U–Pb dating and Hf isotope, major and trace-element geochemistry of the Jiangjunshan and Dakalasu A_2-type granites. These results can be used to constrain their possible emplacement ages, source, and petrogenesis and thus provide important insights into understanding the postcollisional extensional environment of the Chinese Altay orogeny.

2 | REGIONAL GEOLOGY

The Chinese Altay orogenic belt is situated between the southern margin of the Siberian Block and the northern margin of the Kazakhstan–Junggar Block, bounded to the northwest by the Rudny Altay of Kazakhstan and the Gorny Altay of Russia, to the southeast by Gobi Altay of Mongolia, and separated from the Junggar Basin by the Erqis Fault (Li, Yang, Li, Santosh, Chen, & Xiao, 2014b; Xiao & Santosh, 2014; Zhang, Chen, Zheng, Qin, & Li, 2014b; Zheng et al., 2014). Northwest (NW)-trending faults are widely developed in the Chinese Altay orogen, such as the Hongshanzui Fault, Abagong Fault, Tesibahan Fault, and Erqis Fault. Based on the context of stratigraphic, metamorphic, deformation, and magmatic features, five or six terranes or tectonic units have been distinguished in the Chinese Altay, which are separated by these NW-trending faults (Figure 1; Windley et al., 2002).

Terrane 1 largely comprises Middle to Late Devonian andesite and dacite and Late Devonian to Early Carboniferous lower greenschist facies metasediments, including shale, siltstone, greywacke, sandstone, and limestone. Terrane 2 consists predominantly of thick Neoproterozoic to Middle Ordovician sedimentary rocks that include turbidites of the Habahe Group, with minor Early Devonian sedimentary and volcanic rocks. Rocks of the Habahe Group are isoclinally folded and metamorphosed at lower greenschist facies. Terrane 3 constitutes the central part of the Chinese Altay orogen and is mainly formed from Neoproterozoic to Middle Ordovician turbidite and continental sedimentary rocks metamorphosed at greenschist to upper amphibolite facies conditions. Terrane 4 is mainly composed of the Late Silurian to Early Devonian Kangbutiebao Formation and the overlying Middle Devonian Altay Formation. The terrane includes

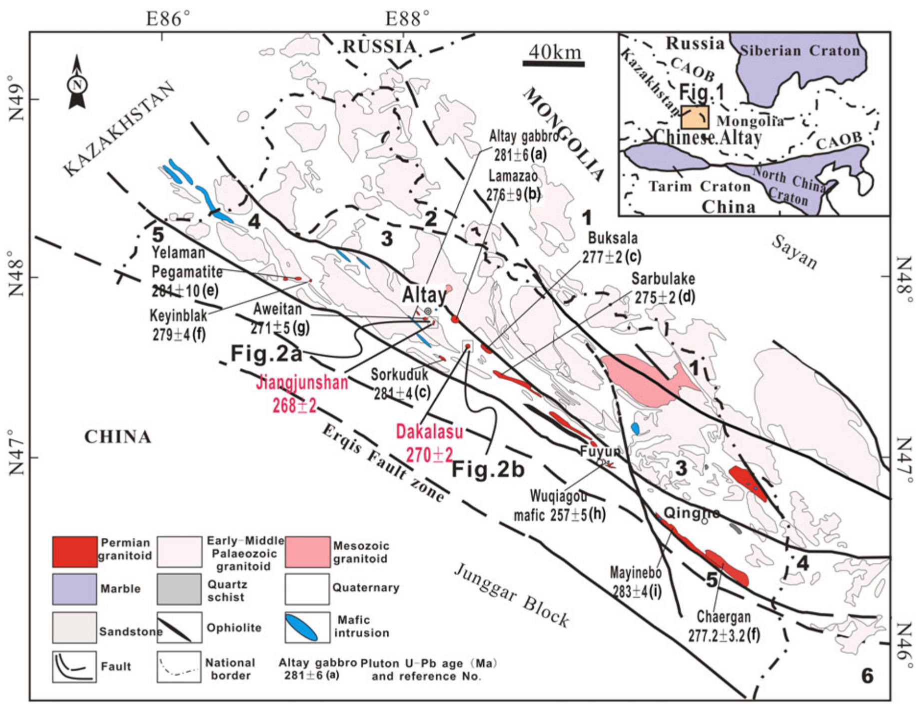

FIGURE 1 Simplified geological map of the Chinese Altay. Tectonic subdivision modified from Windley et al. (2002). Permian intrusions are marked by their zircon ages. Data sources: (a), Tong et al. (2006); (b) Wang et al. (2005); (c) Gao et al. (2010); (d) Sun, Li, Yang, Li, Zhu, & Yang (2009a); (e) Sun et al., 2009b; (f) Zhang et al. (2010); (g) Tong et al. (2014b); (h) Chen and Han (2006); (i) Zhang et al. (2012) [Colour figure can be viewed at wileyonlinelibrary.com]

metamorphic rocks with greenschist to upper amphibolite and locally granulite facies assemblages (Wei, Clarke, Tian, & Qiu, 2007). Xu et al. (2003) reported an ophiolite sequence dominated by mafic rocks with mid-ocean ridge basalt (MORB) affinity in the Kuerti area at the central part of the terrane and inferred that they formed in a back-arc basin environment. Terrane 5 is largely composed of Early Palaeozoic to Devonian sedimentary rocks and Late Carboniferous volcanoclastic rocks, metamorphosed at greenschist to amphibolite facies conditions. Terrane 6 consists entirely of Devonian island-arc rocks with small amounts of Ordovician limestones and some Carboniferous island-arc volcanics. This terrane belongs to the Junggar Block and was separated from the Altay orogen (Terrane 5) by the Erqis Fault, one of the largest transcurrent faults in Central Asia (Sengör et al., 1993).

Granitic rocks occupy at least 40% of the Chinese Altay (Figure 1) and some highly deformed and metamorphosed rocks are identified as orthogneiss or gneissic granite. Recently, precise zircon U–Pb data have shown that most of the granitic intrusions have Early to Middle Palaeozoic ages (Briggs et al., 2007; Cai, Sun, Yuan, Zhao, Xiao, Long, & Wu, 2011a; Sun et al., 2008; Wang et al., 2006; Windley et al., 2002; Yuan et al., 2007). In contrast, Late Palaeozoic and Mesozoic plutonism was found to be relatively weak with limited distribution. For instance, Yuan et al. (2007) reported an I-type granitic pluton with a zircon U–Pb age of 318 ± 6 Ma and suggested that it was emplaced during the waning period of magmatic activity. Many small A-type granitic plutons have emplacement ages of ca. 300–270 Ma, and massive pegmatite dykes were emplaced in the period of 280–205 Ma (Ren, Zhang, Tang, & Lv, 2011; Shen, Zhang, Wang, Wyman, & Yang, 2011; Tong, Tao, Kovach, Hong, & Han, 2006; Wang et al., 2007).

3 | SAMPLES AND ANALYTICAL METHODS

3.1 | Analysis of chemical compositions of the granite

Twelve whole-rock samples were collected from surface exposures; the sample locations are shown in Figure 2a and 2b. All samples were trimmed to remove the altered surfaces and crushed and powdered with an agate mill.

Major element compositions were analyzed with a PANanalytical Axios x-ray fluorescence (XRF) spectrometer at ALS Chemex (Guangzhou) Co, Ltd. A quantity of 0.9 g of the sample was added to 9.0 g of lithium borate flux (50% $Li_2B_4O_7$–50% $LiBO_2$), mixed well and fused in an auto fluxer between 1,050 and 1,100 °C. A flat molten glass disc was prepared from the resulting melt. This disc was analyzed by XRF spectrometry. The precision of XRF analyses at ALS Chemex was 2%.Trace-element concentrations were determined with an Elan 9000 ICP-MS at the same laboratory. A prepared sample (0.2 g) was added to the lithium metaborate flux (0.9 g), mixed well and fused in a furnace at 1,000 °C. The resulting melt was then cooled and dissolved in 100 ml of 4% HNO_3. This solution was then analyzed by inductively coupled plasma-mass spectrometry (ICP-MS). The precision of the ICP-MS analyses at ALS Chemex was better than 10% for all elements. Whole-rock chemical composition data are reported as weight percent (wt%), and trace-element and rare earth element

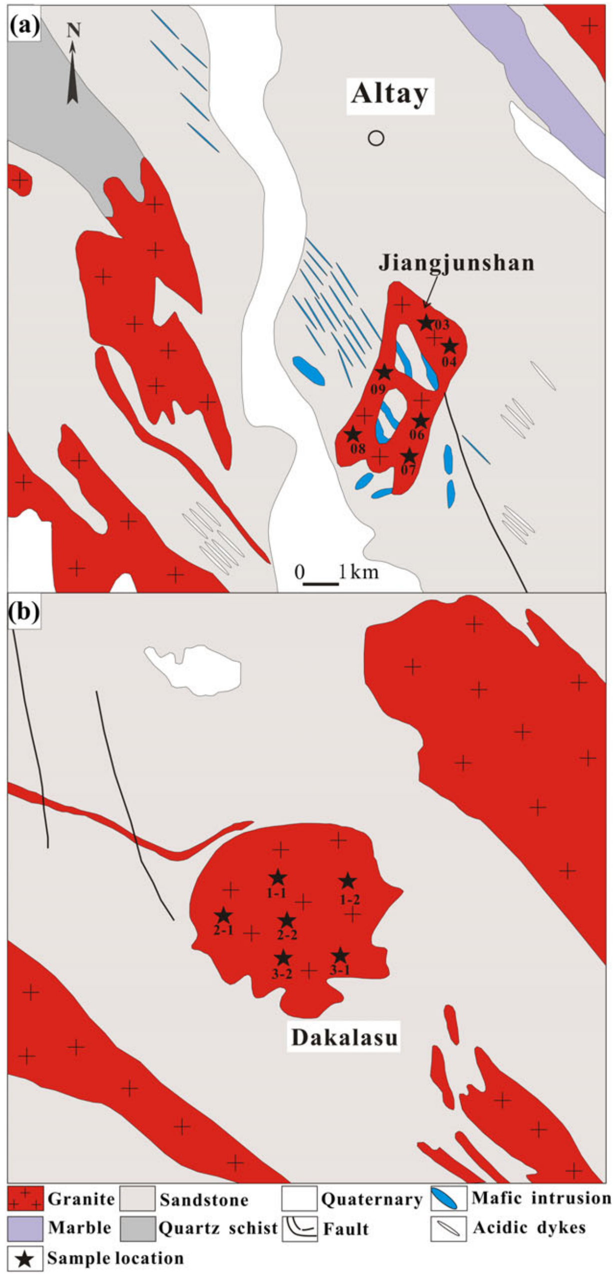

FIGURE 2 More detailed map showing sampling location of the (a) Jiangjunshan and (b) Dakalasu granite plutons [Colour figure can be viewed at wileyonlinelibrary.com]

(REE) data are reported in parts per million (10^{-6}). The analytical results are listed in Table 1.

3.1.1 | Zircon U–Pb dating by LA-ICP-MS

Zircon grains from Jiangjunshan and Dakalasu granites were separated using conventional heavy liquid and magnetic techniques. After the hand-picked zircon grains were cleaned with an acid bath, they were mounted in epoxy blocks and then polished to obtain a smooth surface. The selection of zircon grains for isotopic analysis was based upon cathodoluminescence images (Figure 3). The U–Pb dating of zircon was conducted by laser ablation ICP-MS (LA-ICP-MS) at the State Key Laboratory of Ore Deposit Geochemistry, Institute of Geochemistry, Chinese Academy of Sciences, Guiyang. A GeoLasPro laser ablation system (LamdaPhysik, Gottingen, Germany) and an Agilent

TABLE 1 Major oxides (wt%) and trace element (ppm) compositions of the Jiangjunshan alkali-feldspar granite and Dakalasu alkali-feldspar granite in the southern Altay Range

	Jiangjunshan alkali-feldspar granite						Dakalasu alkali-feldspar granite					
Sample no.	JJS-13-03	JJS-13-04	JJS-13-06	JJS-13-07	JJS-13-08	JJS-13-09	KLS-13-1-1	KLS-13-1-2	KLS-13-2-1	KLS-13-2-2	KLS-13-3-1	KLS-13-3-2
Major oxides												
SiO_2	72.95	72.05	73.27	72.4	72.38	72.48	70.69	70.57	70.14	69.55	71.04	70.61
Al_2O_3	13.85	14.22	13.92	13.98	13.9	14.1	14.44	14.15	14.6	14.68	14.37	14.59
Fe_2O_3	2.04	1.93	1.86	2.02	2	1.88	3.01	3.19	3.18	2.93	2.8	2.25
MgO	0.34	0.34	0.32	0.34	0.35	0.32	0.79	0.67	0.93	0.6	0.76	0.56
CaO	1.05	0.99	1.01	1.15	1.15	1.09	1.99	1.55	2.14	1.59	1.81	1.49
Na_2O	3.46	3.43	3.66	3.71	3.56	3.63	4.6	3.4	4.13	3.9	3.55	3.53
K_2O	4.97	5.26	4.83	4.75	4.85	5.07	2.64	4.92	3.2	4.48	4.44	5.13
MnO	0.1	0.05	0.06	0.05	0.05	0.05	0.07	0.06	0.05	0.05	0.05	0.04
P_2O_5	0.14	0.14	0.12	0.14	0.14	0.14	0.266	0.214	0.319	0.193	0.267	0.17
TiO_2	0.21	0.21	0.2	0.22	0.22	0.21	0.43	0.5	0.47	0.46	0.4	0.37
LOI	0.92	0.82	0.71	0.58	0.7	0.63	0.54	0.59	0.43	0.56	0.54	0.47
Total	100.05	99.48	99.99	99.37	99.33	99.63	99.55	99.9	99.67	99.06	100.1	99.28
A/CNK	1.07	1.08	1.06	1.05	1.05	1.05	1.03	1.03	1.03	1.04	1.03	1.04
A/NK	1.25	1.25	1.24	1.24	1.25	1.23	1.25	1.25	1.24	1.24	1.25	1.23
$K_2O + Na_2O$	8.43	8.69	8.49	8.46	8.41	8.70	7.24	8.32	7.33	8.38	7.99	8.66
Na_2O/K_2O	0.7	0.65	0.76	0.78	0.73	0.72	1.74	0.69	1.29	0.87	0.80	0.69
Trace elements												
Li	103	127	151.5	139	120.5	114.5	210	141.5	187.0	134.5	119.5	94.1
Be	6.5	9.66	7.25	6.13	6.64	11.8	7.34	3.91	5.63	4.39	3.40	3.23
Ga	26.4	25.1	28.1	26.2	24	24.6	22.1	22.5	19.05	21.2	19.60	19.65
Ge	0.22	0.2	0.21	0.22	0.21	0.21	0.20	0.17	0.23	0.20	0.24	0.30
Rb	325	313	386	314	284	311	303	181.5	303	237	182.0	195.0
Sr	63.7	69	61	67.7	70.3	71.8	158.5	144.0	195.0	141.0	147.0	146.0
Y	51.9	50.9	41.7	47.7	47.6	46.2	38.6	36.9	37.3	31.0	39.7	40.8
Zr	75.7	81	76.9	75.3	74.7	73	114.0	40.9	114.0	38.4	94.5	34.7
Nb	30.8	30.6	22.7	29.9	29.6	29.4	18.5	17.5	13.8	16.6	15.9	12.8
Cs	19.05	22.4	23.6	28.1	20.6	30.2	96.7	25.4	48.4	39.5	19.05	13.50
Ba	250	240	220	220	230	250	570	630	780	570	550	560
La	57.1	59.8	54.8	54.7	55.2	52.7	80.7	46.0	64.6	38.3	63.0	129.0
Ce	114	116	109	109	111	104	159.0	87.5	129.0	70.7	120.0	251
Pr	14.3	15	14.3	13.85	13.95	13.45	19.25	10.65	15.20	8.46	14.20	28.6
Nd	55.3	57.6	55	53.9	53.4	51.9	73.4	40.9	56.6	32.0	52.7	104.5
Sm	12.3	12.85	12.6	11.85	11.95	11.5	14.00	8.41	11.20	6.61	10.50	18.55
Eu	0.84	0.93	0.79	0.89	0.92	0.9	1.83	1.95	1.69	1.91	1.52	1.91
Gd	10.45	10.85	9.8	10.25	10.2	10.05	9.92	6.87	9.61	5.98	8.69	12.10
Tb	1.72	1.79	1.55	1.68	1.7	1.63	1.42	1.13	1.48	0.98	1.38	1.79
Dy	8.84	9.14	7.58	8.68	8.73	8.66	7.07	6.21	7.21	5.17	6.95	8.51
Ho	1.73	1.78	1.38	1.68	1.68	1.65	1.38	1.30	1.34	1.05	1.37	1.50
Er	4.72	4.85	3.84	4.47	4.56	4.52	3.75	3.52	3.46	2.99	3.64	3.69
Tm	0.74	0.74	0.61	0.7	0.69	0.69	0.56	0.52	0.47	0.44	0.55	0.51
Yb	4.58	4.66	4.02	4.23	4.33	4.34	3.56	3.19	2.78	2.68	3.37	2.98
Lu	0.68	0.71	0.63	0.65	0.66	0.66	0.57	0.48	0.44	0.43	0.52	0.46
Hf	2.9	3	3.3	2.8	2.7	2.6	3.1	1.1	2.9	1.0	2.4	1.0
Ta	3.56	4.02	3.49	2.53	3.2	5.08	1.30	1.06	0.71	1.13	1.18	1.03
Th	24.6	23.5	23.9	23.2	23.7	22.3	40.1	9.1	33.7	10.1	28.5	37.4
U	3	4.7	2.5	9.5	3.5	3.2	8.9	2.4	3.1	1.4	1.4	2.1
Y/Nb	1.69	1.66	1.84	1.6	1.61	1.57	2.09	2.11	2.70	1.87	2.50	3.19

(*Continues*)

TABLE 1 (Continued)

Sample no.	JJS-13-03	JJS-13-04	JJS-13-06	JJS-13-07	JJS-13-08	JJS-13-09	KLS-13-1-1	KLS-13-1-2	KLS-13-2-1	KLS-13-2-2	KLS-13-3-1	KLS-13-3-2
	Jiangjunshan alkali-feldspar granite						Dakalasu alkali-feldspar granite					
Yb/Ta	1.29	1.16	1.15	1.67	1.35	0.85	2.74	3.01	3.92	2.37	2.86	2.89
Ba/La	4.38	4.01	4.01	4.02	4.17	4.74	7.06	13.70	12.07	14.88	8.73	4.34
Zr/Nb	2.46	2.65	3.39	2.52	2.52	2.48	6.16	2.34	8.26	2.31	5.94	2.71
Rb/Sr	5.1	4.54	6.33	4.64	4.04	4.33	1.91	1.26	1.55	1.68	1.24	1.34
Eu/Eu*	0.22	0.23	0.21	0.24	0.25	0.25	0.45	0.76	0.49	0.91	0.47	0.37
Ba/Nb	8.12	7.84	9.69	7.36	7.77	8.5	30.81	36.00	56.52	34.34	34.59	43.75
(La/Sm)N	3	3	2.81	2.98	2.98	2.96	3.72	3.53	3.72	3.74	3.87	4.49
Ba/Th	10.16	10.21	9.21	9.48	9.7	11.21	14.21	69.23	23.15	56.44	19.30	14.97
Th/Yb	5.37	5.04	5.95	5.48	5.47	5.14	11.26	2.85	12.12	3.77	8.46	12.55
U/Pb	0.04	0.1	0.04	0.19	0.07	0.06	0.21	0.06	0.10	0.03	0.03	0.05
Nb/U	10.27	6.51	9.08	3.15	8.46	9.19	2.08	7.29	4.45	11.86	11.36	6.10
Ce/Nb	3.69	3.79	4.78	3.65	3.75	3.54	8.59	5.00	9.35	4.26	7.55	19.61
Hf/Nb	0.09	0.1	0.15	0.09	0.09	0.09	0.17	0.06	0.21	0.06	0.15	0.08
Sr/Y	1.23	1.36	1.46	1.42	1.48	1.55	4.11	3.90	5.23	4.55	3.70	3.58
ΣREE	286.8	296.7	275.4	276.53	278.97	266.65	376.41	218.63	305.08	177.70	288.39	565.10

Note. REE = rare earth element.

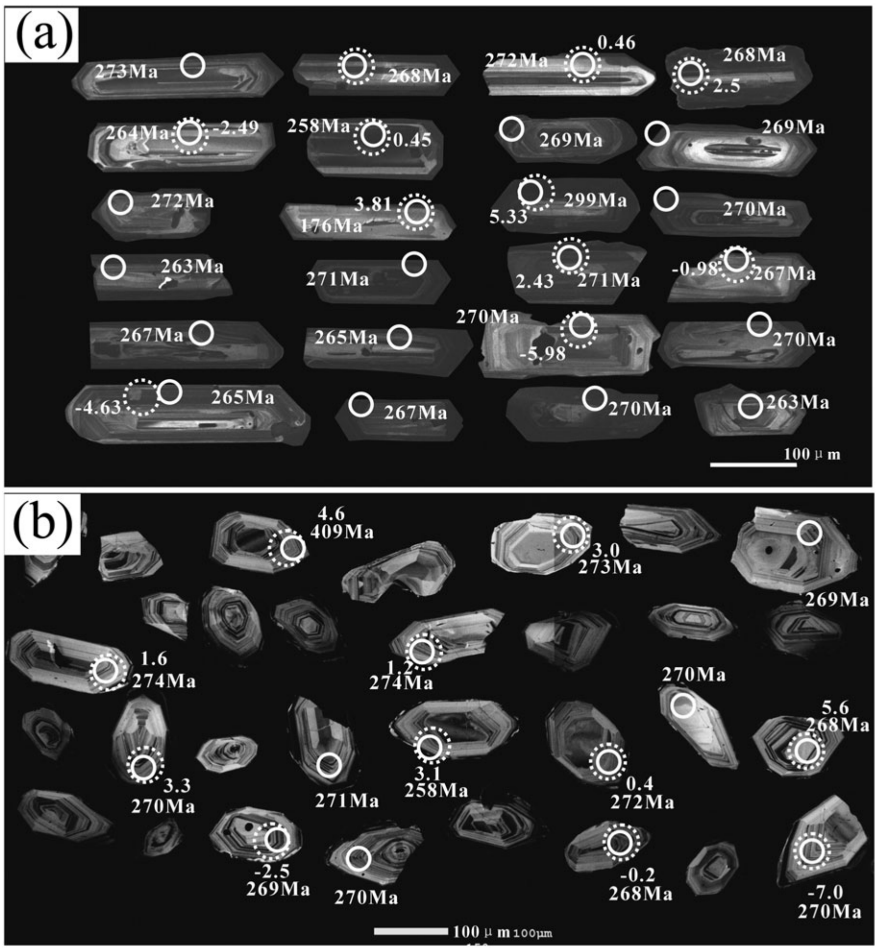

FIGURE 3 Representative cathodoluminescence images for zircons from the (a) Jiangjunshan and (b) Dakalasu granites

7700× ICP-MS system (Agilent Technologies, Tokyo, Japan) were combined for these measurements. A 193-nm ArF excimer laser, homogenized by a set of beam delivery systems, was focused on a zircon surface with a flux of 10 J/cm^2. The ablation protocol employed a spot diameter of 32 μm at a 5-Hz repetition rate for 40 s (equating to 200 pulses). Helium was applied as a carrier gas to efficiently transport the aerosol to the ICP-MS system. Zircon 91500 was used as an external standard to correct instrumental mass discrimination and elemental fractionation. Zircon GJ-1 and Plešovice were treated as quality control references for geochronology. The common lead concentration of zircon was externally calibrated against NIST SRM 610 with Si as an internal standard, whereas Zr served as the internal standard for the other trace elements (Hu et al., 2011; Liu, Gao, Hu, Gao, Zong, & Wang, 2010b). Raw data reduction was performed off-line by ICPMSDataCal (Liu, Gao et al., 2010; Liu, Hu, Zong, Gao, Gao, Xu, & Chen, 2010a).

3.2 | In situ zircon Hf isotope analysis

Zircon Hf isotopic analyses were performed on a Nu Plasma HR MC-ICP-MS (Nu Instruments Ltd., UK) equipped with a GeoLas 2005 193-nm ArF excimer laser ablation system at the State Key Laboratory of Continental Dynamics, Northwest University, Xi'an, P.R. China. Analyses were conducted using a spot size of 44 μm, and He was used as the carrier gas. The laser repetition rate was 10 Hz, and the energy density applied was 15–20 J/cm^2. Raw count rates for ^{172}Yb, ^{173}Yb, ^{175}Lu, ^{176}(Hf + Yb + Lu), ^{177}Hf, ^{178}Hf, ^{179}Hf, and ^{180}Hf were collected simultaneously. The isobaric interference of ^{176}Lu on ^{176}Hf was corrected by measuring the intensity of an interference-free ^{175}Lu isotope, and a recommended ^{176}Lu/^{175}Lu ratio of 0.02669 was used to calculate ^{176}Lu/^{177}Hf. Similarly, the interference of ^{176}Yb on ^{176}Hf was corrected by measuring an interference-free ^{172}Yb isotope and using a ^{176}Lu/^{172}Yb ratio of 0.5886 to calculate ^{176}Hf/^{177}Hf ratios (Chu et al., 2002). Time-dependent drifts of Lu–Hf isotopic ratios were corrected using linear interpolation according to the variations of 91500 and GJ-1. To evaluate the data quality, we reanalyzed 91500 and GJ-1 as unknown. The obtained ^{176}Hf/^{177}Hf ratios were 0.282295 ± 0.000027 (n = 14, 2σ) for 91500 and 0.282734 ± 0.000015 (n = 16, 2σ) for GJ-1. These results are in good agreement with the recommended ^{176}Hf/^{177}Hf ratio within 2σ (0.2823075 ± 58, 2σ and 0.282015 ± 0.000019, 2σ; Griffin, Pearson, Belousova, & Saeed, 2006; Wu, Yang, Xie, Yang, & Xu, 2006).

A decay constant for ^{176}Lu of 1.865 × 10^{-11}a^{-1} (Scherer, Munker, & Mezger, 2001) and present-day chondritic ratios of ^{176}Hf/^{177}Hf = 0.282772 and ^{176}Lu/^{177}Hf = 0.0332 (Blichert-Toft & Albarède, 1997) were adopted to calculate the initial values of ^{176}Hf/^{177}Hf and $\varepsilon_{Hf}(t)$. Depleted mantle Hf model ages (T_{DM}) were calculated from the measured ^{176}Lu/^{177}Hf and ^{176}Hf/^{177}Hf ratios of the zircons, assuming a present-day ^{176}Hf/^{177}Hf ratio of 0.283250 and a ^{176}Lu/^{177}Hf ratio of 0.0384 for the depleted mantle (Griffin et al., 2002). The average crustal ^{176}Lu/^{177}Hf value of 0.015 was adopted to calculate the two-stage model ages (Griffin et al., 2002).

4 | RESULTS

4.1 | Petrography

The Jiangjunshan pluton is located 4 km southeast of Altai city and intrudes into the Devonian Altai Formation. The main rock of this pluton is K-feldspar granite. The granite samples are light grey with coarse-grained inequigranular texture (Figure 4a). The major minerals are K-feldspar (60–70 vol%), quartz (20–30 vol%), plagioclase (~5 vol%), and biotite (~5 vol%). Accessory minerals include zircon, apatite, and ilmenite. K-feldspar crystals range up to ~10 mm and consist primarily of microcline with a typical tartan twin (Figure 4b). Quartz is subhedral to anhedral, ranging from 0.1 to 2 mm. Plagioclase shows polysynthetic twins with a zone texture. Biotite is fine grained (<0.5 mm) and typically forms small aggregates.

The Dakalusu pluton is situated 6 km northwest of Altai city and also intrudes into the Devonian Altai Formation. The main rock of this pluton is biotite granite. The pluton consists of two main phases that are texturally distinct. Contact between the two phases is gradual,

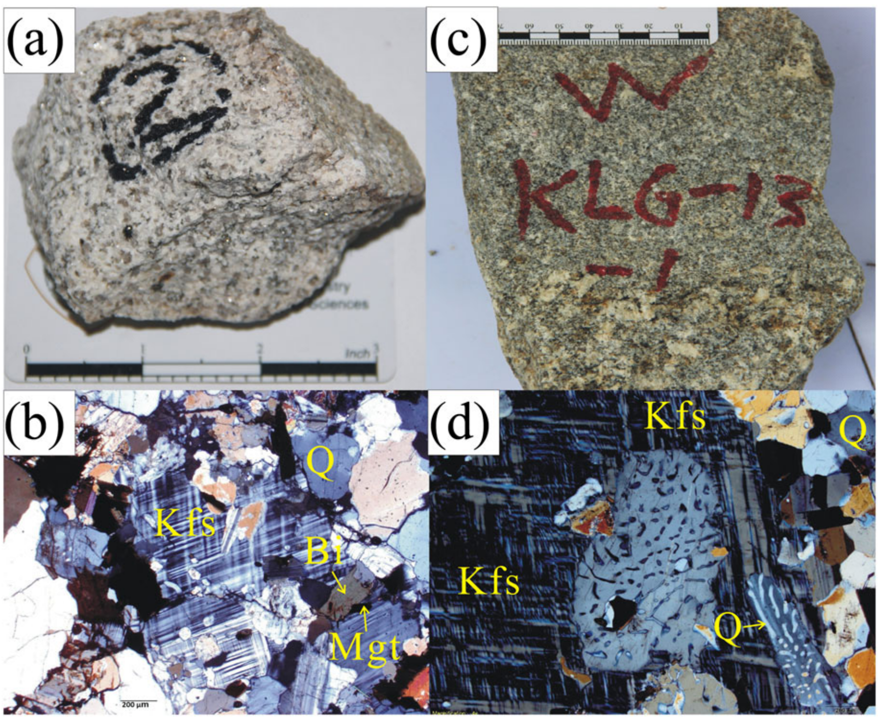

FIGURE 4 Photos of hand specimens of (a) Jiangjunshan granite pluton and (c) Dakalasu granite pluton and petrographic micrographs cross polarized light of (b) Jiangjunshan granite (transmitted, 10 × 5) and (d) Dakalasu granite (transmitted, 10 × 5). Bt = biotite; Kfs = K-feldspar; Mgt = magnetite; Q = quartz [Colour figure can be viewed at wileyonlinelibrary.com]

changing from porphyritic texture to inequigranular texture (Figure 4c). The two phases are consistent with the size and number of the K-feldspar phenocryst and have a similar mineral composition: (30–40 vol%), albite (20–30 vol%), quartz (20–30 vol%), plagioclase (5–10 vol%), and biotite (~5 vol%). K-feldspar is mainly microcline. Microcline crystals usually occur as phenocrysts in porphyritic granite with grain diameters up to 20 mm. In contrast, microcline grains are usually <7 mm in size and are locally abundant or aggregated in inequigranular granite. Microcline crystals have typically cross-hatched twins (Figure 4d). Albite is anhedral and 0.05 to 0.6 mm in size. Myrmekitic texture is commonly seen in the thin section (Figure 4d). Quartz is anhedral and ranges from 0.2 to 0.5 mm in size. Plagioclase occurs as medium-acid plagioclase and has a polysynthetic twin. Biotite is irregularly flaky with a flake size of 0.1–0.5 mm in diameter.

4.2 | Major and trace-element composition

The major and trace-element composition of the Jiangjunshan and Dakalasu granites is listed in Table 1. The Jiangjunshan granite exhibits a high content of SiO_2 (varying from 72.05 to 73.27 wt%), Al_2O_3 (varying from 13.85 to 14.22 wt%), and total alkali ($Na_2O + K_2O$, from 8.41 to 8.71 wt%) and a low CaO content (from 0.99 to 1.05 wt%). The Dakalasu granite shows a high content of SiO_2 (varying from 69.55 to 71.04 wt%), Al_2O_3 (varying from 14.15 to 14.68 wt%), and total alkali ($Na_2O + K_2O$, from 7.24 to 8.66 wt%) and low CaO content (from 1.49 to 2.14 wt%). On the quartz-alkali feldspar-plagioclase feldspar (QAP) classification diagrams, the granites are classified as alkali-feldspar granite (Figure 5a). All samples are plotted in the subalkalic granite field in the ($K_2O + Na_2O$) versus SiO_2 discrimination diagram (Figure 5 b), and the high-K calc alkaline is plotted in the shoshonite series field in the K_2O versus SiO_2 diagram (Figure 5c). The Jiangjunshan and Dakalasu alkali-feldspar granites are weak peraluminous, with A/CNK (molar ratio of $Al_2O_3/[CaO + Na_2O + K_2O]$) ratios ranging from 1.05 to 1.08 and 1.03 to 1.08 (Table 1 and Figure 5d), respectively. The granites have a relatively high Fe_2O_3 content (1.86–2.04 wt% for the Jiangjunshan granite and 2.25–3.19 wt% for the Dakalasu granite) and low MgO content (0.32–0.35 wt% for the Jiangjunshan granite and 0.56–0.93 wt% for the Dakalasu granite). FeO^T/MgO ratios of the Jiangjunshan and Dakalasu granites vary from 5.67 to 6.02 with an average of 5.83 and from 3.42 to 4.88 with an average of 4.10, respectively, which are clearly higher than those of I-type granites (average of 2.27 from 991 samples) and S-type granites (average of 2.38 from 578 samples; Whalen et al., 1987).

The total REE content of the Jiangjunshan granite and Dakalasu granite varies from 266.65 to 269.70 ppm and 177.70 to 565.10 ppm, respectively. The chondrite-normalized REE pattern of the Jiangjunshan granite shows a relative enrichment of light rare earth elements, with $(La/Yb)_N$ ratios varying from 8.71 to 9.78 and large negative Eu anomalies (δEu = 0.21–0.25; Figure 6a and 6c). The larger $(La/Yb)_N$ ratios, $(La/Yb)_N$ = 10.25–31.05, and δEu values (δEu = 0.37–0.91) of the Dakalasu granite also indicate an enrichment of light rare earth element and weakly negative Eu anomalies.

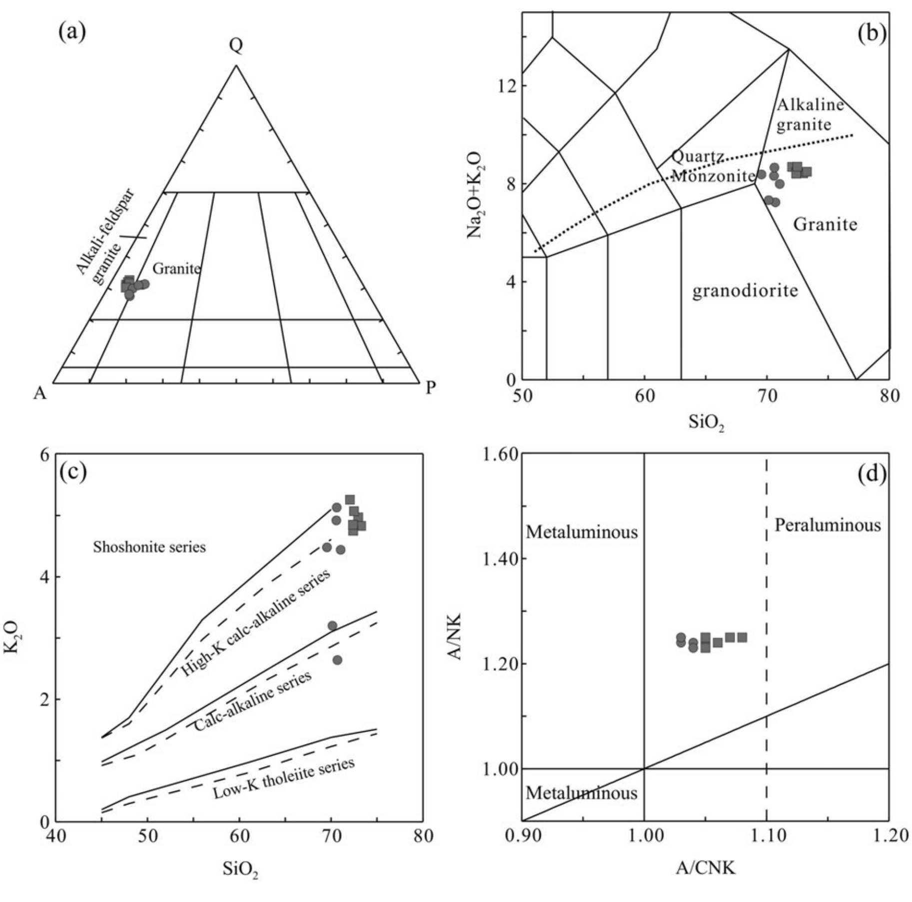

FIGURE 5 Chemical classification diagrams for the Jiangjunshan and Dakalasu alkali-feldspar granites: (a) QAP diagram (Streckeisen, 1974); (b) total alkalis ($K_2O + Na_2O$) versus SiO_2 diagram (compositional fields from Middlemost, 1994); (c) K_2O versus SiO_2 diagram; and (d) A/NK versus A/CNK diagram (Maniar & Piccoli, 1989)

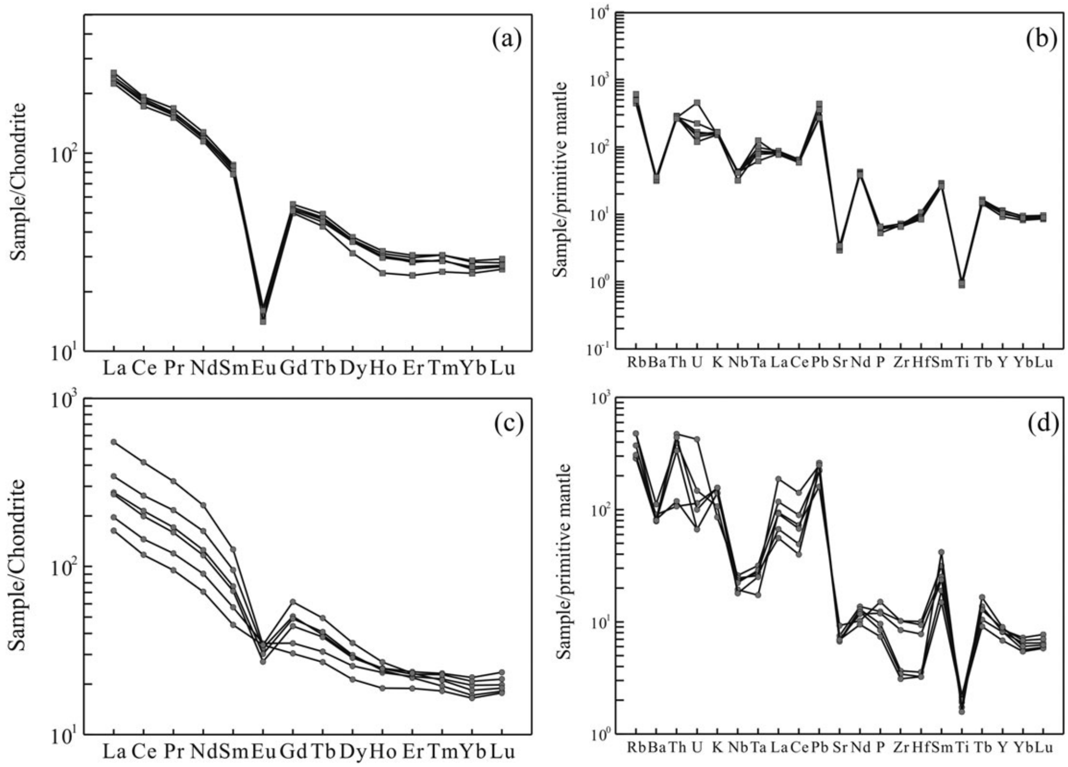

FIGURE 6 Primitive mantle-normalized extended trace-element spidergram patterns for the (a) Jiangjunshan and (c) Dakalasu alkali-feldspar granites and chondrite-normalized rare earth element patterns for the (b) Jiangjunshan and (d) Dakalasu alkali-feldspar granites. Data of primitive mantle and chondrite are from Sun & McDonough (1989)

The Jiangjunshan and Dakalasu granites are characterized by a high content of high-field strength elements, such as Ta, Zr, Hf, and Th. The high Ga/Al ratios of the Jiangjunshan and Dakalasu granites with a 10,000 × Ga/Al value that ranges from 2.62 to 4.19 indicate that they are geochemically similar to A-type granites. In the primitive mantle-normalized spider diagram (Figure 6b and 6d), the granites exhibit strongly negative Ba, Sr, Ti, and Eu anomalies and slightly negative Nb anomalies.

4.3 | Zircon U–Pb geochronology

Zircon grains from the Jiangjunshan and Dakalasu granites are pale yellow, euhedral, and tetragonal dipyramidal. The grain size of zircons ranges from 100 to 200 μm with elongation ratios (c/a) ranging from 2 to 4. In cathodoluminescence images (Figure 4), most zircon grains display fine oscillatory zonation, which is a typical of magmatic zircon. The U–Pb isotope analytical results for 39 spots are listed in Table 2.

Twenty-four spot analyses of zircons from the Jiangjunshan granite show that they contain 240–1,619 ppm U and 61–682 ppm Th, with Th/U ratios varying from 0.25 to 0.42. Two spots yielded a relatively younger $^{206}Pb/^{238}U$ age (176 and 258 Ma), and one spot yielded relatively older $^{206}Pb/^{238}U$ ages (299 Ma). The other 21 spots have similar $^{206}Pb/^{238}U$ ages and give a weighted mean age of 268.3 ± 1.9 Ma (Figure 7a), which is regarded as the best estimate for the emplacement age of the Jiangjunshan granite.

Fifteen spots of zircons from the Dakalasu granite were analyzed. These spots yielded $^{206}Pb/^{238}U$ ages from 258 to 274 Ma, with a weighted mean age of 270.4 ± 1.9 Ma (Figure 7b), except that one spot yielded a $^{206}Pb/^{238}U$ age of 409 Ma. Thus, we suggest that 270.4 ± 1.9 Ma represents the best estimate for their emplacement age.

4.4 | In situ zircon Hf isotope

The in situ Hf isotope analyses of the Jiangjunshan and Dakalasu granites are listed in Table 3. The $^{176}Lu/^{177}Hf$ ratios of most zircons are lower than 0.0025, suggesting that the zircons accumulated little radiogenic Hf after they formed; therefore, the $^{176}Hf/^{177}Hf$ ratios represent the isotopic composition of the zircons when they crystallized (Patchett et al., 1981; Knudsen, Griffin, Hartz, Andresen, & Jackson, 2001; Kinny & Maas, 2003). The $^{206}Pb/^{238}U$ ages of the zircon grains were used to calculate the initial $^{176}Hf/^{177}Hf$ ratios and $\varepsilon_{Hf}(t)$. Twelve spots on zircons were analyzed for each of Jiangjunshan and Dakalasu, yielding variable $\varepsilon_{Hf}(t)$ values of −6.0 to +5.3 and −7.0 to +5.6, respectively. The yielded two-stage (T_{DM2}) model ages generally vary from 1.60 to 2.44 Ga (an average of 1.99 Ga) and 1.58 to 2.50 Ga (an average of 1.91 Ga), respectively.

5 | DISCUSSION

5.1 | Age of the Jiangjunshan and Dakalasu alkali-feldspar granites

The Jiangjunshan alkali-feldspar granite has been identified as a Jurassic granite complex (~151 Ma) using whole-rock Rb–Sr isotope data (Chen & Jahn, 2002) and by zircon U–Pb dating of 13 spots from one

TABLE 2 Zircon LA-ICP-MS U–Pb data of the Jiangjunshan alkali-feldspar granite and Dakalasu alkali-feldspar granite in the southern Altay Range

No.	Pb (ppm)	Th (ppm)	U (ppm)	Th/U	$^{207}Pb/^{206}Pb$		$^{207}Pb/^{235}U$		$^{206}Pb/^{238}U$		$^{207}Pb/^{206}Pb$		$^{207}Pb/^{235}U$		$^{206}Pb/^{238}U$	
					Ratio	1σ	Ratio	1σ	Ratio	1σ	Age (Ma)	1σ	Age (Ma)	1σ	Age (Ma)	1σ
Jiangjunshan																
1	12.1	143.9	245.5	0.59	0.05783	0.00330	0.33171	0.01759	0.04172	0.00083	524	124	291	13	263	5
2	20.7	252.5	391.8	0.64	0.05706	0.00271	0.34005	0.01520	0.04279	0.00085	494	104	297	12	270	5
3	8.3	85.5	167.2	0.51	0.05510	0.00289	0.31718	0.01586	0.04235	0.00079	417	117	280	12	267	5
4	40.0	353.3	797.5	0.44	0.06447	0.00234	0.38775	0.01340	0.04277	0.00056	767	76	333	10	270	3
5	10.7	94.7	205.9	0.46	0.07392	0.00392	0.42738	0.02186	0.04254	0.00086	1039	107	361	16	269	5
6	19.0	204.3	381.8	0.53	0.05768	0.00281	0.33803	0.01527	0.04246	0.00065	517	107	296	12	268	4
7	79.6	575.8	1645.0	0.35	0.06720	0.00220	0.40506	0.01210	0.04273	0.00067	844	67	345	9	270	4
8	26.7	283.2	525.2	0.54	0.05128	0.00204	0.30753	0.01186	0.04275	0.00062	254	88	272	9	270	4
9	19.7	206.3	396.0	0.52	0.05013	0.00222	0.29835	0.01253	0.04288	0.00059	211	104	265	10	271	4
10	63.9	425.4	1096.2	0.39	0.07987	0.00272	0.53752	0.01830	0.04751	0.00059	1194	68	437	12	299	4
11	24.0	232.1	490.5	0.47	0.05149	0.00283	0.30632	0.01487	0.04269	0.00067	261	126	271	12	269	4
12	11.3	61.1	240.2	0.25	0.04928	0.00357	0.29759	0.02111	0.04308	0.00091	161	163	265	17	272	6
13	18.0	198.1	356.1	0.56	0.04981	0.00269	0.29059	0.01468	0.04222	0.00073	187	126	259	12	267	5
14	39.8	376.2	786.9	0.48	0.06089	0.00240	0.35711	0.01310	0.04204	0.00067	635	83	310	10	265	4
15	80.6	681.7	1619.4	0.42	0.05872	0.00208	0.35148	0.01108	0.04286	0.00058	567	78	306	8	271	4
16	58.3	306.3	1559.5	0.20	0.13077	0.00523	0.49828	0.01790	0.02768	0.00066	2109	70	411	12	176	4
17	33.7	578.5	642.5	0.90	0.05116	0.00230	0.29107	0.01237	0.04076	0.00068	256	104	259	10	258	4
18	58.0	313.0	1161.4	0.27	0.07762	0.00318	0.46322	0.01818	0.04247	0.00065	1139	81	386	13	268	4
19	13.6	173.2	270.3	0.64	0.05217	0.00367	0.29551	0.01841	0.04192	0.00093	300	166	263	14	265	6
20	28.1	247.0	591.4	0.42	0.05176	0.00209	0.30650	0.01157	0.04231	0.00060	276	88	271	9	267	4
21	18.6	304.2	364.7	0.83	0.05160	0.00243	0.29515	0.01277	0.04156	0.00073	333	103	263	10	263	5
22	19.1	199.2	388.1	0.51	0.05007	0.00219	0.30462	0.01323	0.04313	0.00069	198	99	270	10	272	4
23	30.8	256.6	656.4	0.39	0.06137	0.00254	0.35884	0.01364	0.04188	0.00067	654	89	311	10	264	4
24	19.6	180.9	366.1	0.49	0.09158	0.00468	0.54660	0.02402	0.04329	0.00086	1459	98	443	16	273	5
Dakalasu																
1	45.4	589.5	774.6	0.76	0.05190	0.00097	0.31051	0.00642	0.04337	0.00049	280	43	275	5	274	3
2	92.6	873.2	1768.2	0.49	0.05360	0.00099	0.30080	0.00624	0.04077	0.00065	354	36	267	5	258	4
3	100.3	416.3	1971.0	0.21	0.05276	0.00087	0.31611	0.00595	0.04344	0.00036	317	44	279	5	274	2
4	44.1	175.2	551.0	0.32	0.05504	0.00078	0.49721	0.00852	0.06550	0.00046	413	36	410	6	409	3
5	30.0	511.9	481.3	1.06	0.05328	0.00138	0.31158	0.00954	0.04249	0.00077	343	59	275	7	268	5
6	176.9	630.2	3610.9	0.17	0.05465	0.00120	0.32029	0.01101	0.04273	0.00119	398	55	282	8	270	7
7	18.0	249.8	300.1	0.83	0.06451	0.00211	0.37703	0.01296	0.04265	0.00083	767	70	325	10	269	5
8	107.5	141.1	2219.7	0.06	0.05301	0.00102	0.31094	0.00901	0.04322	0.00138	328	44	275	7	273	8

(*Continues*)

TABLE 2 (Continued)

No.	Pb (ppm)	Th (ppm)	U (ppm)	Th/U	$^{207}Pb/^{206}Pb$ Ratio	1σ	$^{207}Pb/^{235}U$ Ratio	1σ	$^{206}Pb/^{238}U$ Ratio	1σ	$^{207}Pb/^{206}Pb$ Age (Ma)	1σ	$^{207}Pb/^{235}U$ Age (Ma)	1σ	$^{206}Pb/^{238}U$ Age (Ma)	1σ
9	123.7	599.5	2426.8	0.25	0.05395	0.00084	0.31795	0.00685	0.04277	0.00070	369	68	280	5	270	4
10	15.6	173.7	278.6	0.62	0.05361	0.00179	0.31624	0.01125	0.04297	0.00086	354	76	279	9	271	5
11	121.6	259.7	2465.8	0.11	0.06007	0.00084	0.35245	0.00738	0.04262	0.00072	606	30	307	6	269	4
12	87.8	156.6	1788.9	0.09	0.05406	0.00077	0.31964	0.00686	0.04280	0.00056	372	31	282	5	270	3
13	126.1	531.7	2508.6	0.21	0.06682	0.00204	0.38282	0.01017	0.04303	0.00141	831	63	329	7	272	9
14	54.6	466.8	1025.1	0.46	0.05228	0.00097	0.30628	0.00635	0.04249	0.00040	298	43	271	5	268	2
15	119.3	386.8	2516.5	0.15	0.05786	0.00085	0.34352	0.01042	0.04274	0.00089	524	33	300	8	270	5

Note. LA-ICP-MS = laser ablation inductively coupled plasma-mass spectrometry.

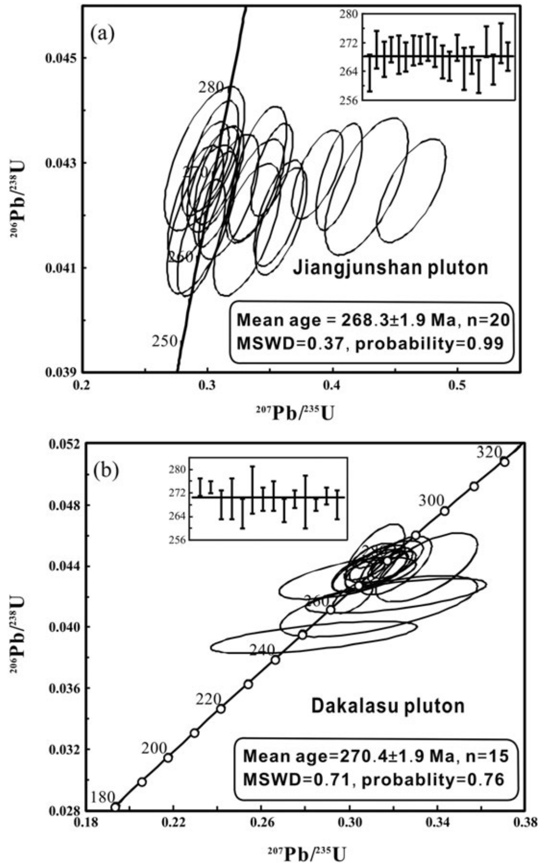

FIGURE 7 Laser ablation inductively coupled plasma-mass spectrometry U-Pb concordant diagrams for zircons from the (a) Jiangjunshan and (b) Dakalasu granites

sample (AT-1) of two-mica monzogranite (Wang, Jahn et al., 2014a). In addition, the Jiangjunshan alkali-feldspar granite has been dated to 220 Ma using muscovite ^{40}Ar–^{39}Ar isotope data (Zhang, Hu, Zhang, Fan, & Pu, 1994) and 235 Ma using whole-rock Rb-Sr isotope data from low ^{87}Rb–^{86}Sr samples (Wang, Zhao, & Zou, 1998). During the long-term evolution of the orogenic belt, the formation and evolution of Altay granite were influenced by multiperiod tectonic activities and magmatism. The isotopic closed system could be sometimes destroyed by magmatism and hydrothermal activities in different periods (Cliff, 1985; Dallmeyer & VanBreeman, 1981; Harrison & McDougall, 1982; Mezger, 1990; Mezger, Hanson, & Bohlen, 1989). Therefore, the age obtained by isotope systems with low closure temperature, such as K–Ar and Ar–Ar methods of potassium-rich mineral (K-feldspar and muscovite), may not accurately represent the real rock-forming age. Zircon U–Pb isotope dating is the best way to determine the granite formation age due to its relatively high closed temperature. In this study, the new LA-ICP-MS zircon U–Pb isotope method was used to confirm the formation age of the Jiangjunshan and Dakalasu alkali-feldspar granites, showing that these granites were emplaced at the Middle Permian (268.3 ± 1.9 and 270.4 ± 1.9 Ma).

Recent studies have established the Permian as one of the most important periods of tectonomagmatic activities in the Chinese Altay. More than 20 Permian granitic plutons have been identified in the past decade (Table 4). Their formation ages range from 290 to 270 Ma, with a peak age of ca. 278 Ma (Tong, Wang et al., 2014). Certain mafic–

TABLE 3 Zircon Lu–Hf isotope data for the Jiangjunshan alkali-feldspar granite and Dakalasu alkali-feldspar granite in the southern Altay Range

Sample	Age (Ma)	$^{176}Hf/^{177}Hf$	1σ	$^{176}Yb/^{177}Hf$	1σ	$^{176}Lu/^{177}Hf$	1σ	$\varepsilon_{Hf}(0)$	$\varepsilon_{Hf}(t)$	T_{DM1}	T_{DM2}	$f_{Lu/Hf}$
Jiangjunshan												
JJS-01	270	0.282719	0.000009	0.030616	0.000359	0.001147	0.000012	−1.9	3.8	758	1714	−0.97
JJS-02	267	0.282587	0.000012	0.049494	0.000360	0.001791	0.000013	−6.6	−1.0	962	2068	−0.95
JJS-03	270	0.282545	0.000012	0.053250	0.000094	0.001926	0.000003	−8.0	−2.5	1026	2180	−0.94
JJS-04	269	0.282487	0.000009	0.068480	0.000323	0.002515	0.000011	−10.1	−4.6	1126	2333	−0.92
JJS-05	268	0.282607	0.000009	0.033780	0.000096	0.001250	0.000003	−5.8	−0.2	919	2015	−0.96
JJS-07	270	0.282629	0.000012	0.056775	0.001295	0.002080	0.000046	−5.1	0.5	909	1957	−0.94
JJS-08	270	0.282761	0.000007	0.024792	0.000463	0.000908	0.000016	−0.4	5.3	694	1602	−0.97
JJS-09	271	0.282627	0.000009	0.050717	0.000572	0.001805	0.000017	−5.1	0.5	903	1960	−0.95
JJS-10	272	0.282681	0.000011	0.039733	0.000868	0.001408	0.000029	−3.2	2.4	817	1816	−0.96
JJS-11	267	0.282684	0.000011	0.041540	0.000140	0.001535	0.000005	−3.1	2.5	817	1809	−0.95
JJS-12	265	0.282447	0.000009	0.060464	0.000250	0.002187	0.000009	−11.5	−6.0	1174	2439	−0.93
Dakalasu												
KLS-10-01-01	270	0.282659	0.000009	0.055497	0.000462	0.002015	0.000016	−4.0	1.6	863	1877	−0.94
KLS-10-01-02	270	0.282701	0.000009	0.022876	0.000101	0.000872	0.000003	−2.5	3.3	778	1766	−0.97
KLS-10-01-03	270	0.282545	0.000010	0.062283	0.000743	0.002200	0.000028	−8.0	−2.5	1033	2181	−0.93
KLS-10-01-04	270	0.282770	0.000010	0.034064	0.000365	0.001258	0.000013	−0.1	5.6	688	1579	−0.96
KLS-10-01-05	270	0.282426	0.000014	0.096272	0.001345	0.003737	0.000053	−12.2	−7.0	1258	2498	−0.89
KLS-10-01-06	270	0.282609	0.000010	0.049007	0.000418	0.001817	0.000013	−5.8	−0.2	930	2011	−0.95
KLS-10-1-08	270	0.282623	0.000007	0.042165	0.000197	0.001655	0.000007	−5.3	0.4	906	1973	−0.95
KLS-10-1-09	270	0.282697	0.000010	0.031561	0.000154	0.001190	0.000005	−2.6	3.1	790	1775	−0.96
KLS-10-1-10	270	0.282645	0.000011	0.041012	0.001000	0.001522	0.000036	−4.5	1.2	872	1916	−0.95
KLS-10-1-11	270	0.282737	0.000009	0.021392	0.000682	0.000778	0.000022	−1.2	4.6	725	1667	−0.98
KLS-10-1-12	270	0.282696	0.000009	0.035148	0.000807	0.001399	0.000031	−2.7	3.0	795	1777	−0.96

ultramafic intrusions, such as the Kalatonke intrusions, were emplaced during 280 to 260 Ma (Chen et al., 2006; Han et al., 2004). In addition to magmatic activities, coeval ultrahigh-temperature metamorphism is also widely distributed in the Chinese Altay. Metamorphism of granulite and paragneiss took place during 295 to 280 Ma, according to the zircon U–Pb ages (Tong, Xu et al., 2014a; Wang, Wei, Wang, Lou, & Chu, 2009; Yang, Li, Liang, & Wang, 2015).

Geographically, most of the plutons or dykes are restricted to being distributed along the NW–SE trending faults at the southern Chinese Altay (Figure 1), and this type of distribution may imply the special origin and tectonic setting for the Permian magmas.

5.2 | Petrogenetic type: A-type affinity

The Jiangjunshan alkali-feldspar granite has high Na_2O + K_2O and high-field strength element content and low CaO, Sr, and Eu content with high FeO^T/MgO and Ga/Al ratio values, exhibiting characteristics of A-type granite (Bonin, 2007; Collins et al., 1982; King et al., 1997; Loiselle & Wones, 1979; Whalen et al., 1987). According to various discrimination diagrams of K_2O/MgO, K_2O + Na_2O, Nb, and Y versus 10,000 Ga/Al, all samples from the Jiangjunshan alkali-feldspar granite and most samples from the Dakalasu alkali-feldspar granite can be plotted in the "A-type granite" field (Eby, 1990; Whalen et al., 1987; Figure 8). Some coeval granites, such as Lamazao granite, Aweitan granite, and Chaergan granite, also show A-type granite affinity (Tong, Wang, et al., 2014; Wang, Hong, Yong, Han, & Shi, 2005; Zhang et al., 2010). These A-type granites, together with the Jiangjunshan and Dakalasu A-type granites recognized in this study, indicate that the Middle Permian represents an important formation period of A-type granites.

In terms of tectonic setting, Eby (1992) divided A-type granites into A_1 and A_2 groups. The A_1 group is associated with mantle-derived magma and emplaced in anorogenic settings, such as hot spots, plumes, or continental rift zones. The A_2 group is derived from underplated mafic magma or melting of continental crust, which is related to postorogenic setting. Using the discrimination diagram of Eby (1992), the Middle Permian A-type granites, including the Jiangjunshan and Dakalasu A-type granites in this study, fall into the A_2 group (Figure 9), suggesting that these granites formed in a postorogenic tectonic setting.

5.3 | Source and petrogenesis

Many compositional variations have been found for A-type granites, and there is no consensus on their origin (Bonin, 2007). A-type granites are genetically diverse and can be produced from various sources and by different processes; thus, several origin models have been proposed, including (a) fractional crystallization of mantle-derived melts (Anderson, Frost, & Frost, 2003; Jiang, Zhang, Zhou, & Liu, 2009; Mansouri Esfahani, Khalili, Kochhar, & Gupta, 2010; Namur et al., 2011), (b) partial melting of crustal rocks (Clemens, Holloway, & White, 1986; Dall'Agnol, Scaillet, & Pichavant, 1999; Whalen et al., 1987), and (c) hybridization between anatectic crustal and mantle-derived magmas (Jung, Mezger, & Hoernes, 1998; Karsli

TABLE 4 Age data of Permian rocks in the Chinese Altay

No.	Location	Rock type	Age (Ma)	Methods	Terrane no.	References
1	Adenbluk	Granite	271 ± 5	Zircon SHRIMP	6	Tong et al., 2014b
2	Aweitan	Granite	271 ± 2	Zircon SHRIMP	4	Tong et al., 2014b
3	Buerjing	Granite	268 ± 5	Zircon SHRIMP	6	Tong et al., 2014b
4	Xibodu	Granite	267 ± 6	Zircon SHRIMP	5	Tong et al., 2014b
5	Daqiaonan	Granite	267 ± 5	Zircon SHRIMP	3	Tong et al., 2014b
6	Altai	Gabbro	281 ± 6	Zircon SHRIMP	4	Tong et al., 2014b
7	Buerjin	Granodiorite	286.3 ± 1.6	Zircon SHRIMP	6	Zhang et al., 2012
8	Fuyun	Granitic dyke	252.2 ± 2.2	Zircon SHRIMP	5	Zhang et al., 2012
9	Fuyun	Migmatite	283 ± 4	Zircon SHRIMP	5	Zhang et al., 2012
10	Buerjing	Keyinblak two-mica granite	278.6 ± 3.5	Zircon LA-ICP-MS	4	Li et al., 2012b
11	Qinghe	Gabbro	272.5 ± 2.4	Zircon SHRIMP	Boundary of 4 and 5	Zhang et al., 2010
12	Dasazi	Bimodal	269.4 ± 2.5	Zircon SHRIMP	3	Zhang et al., 2010
13	Chaergan	Granite	277.2 ± 3.2	Zircon SHRIMP	Boundary of 4 and 5	Zhang et al., 2010
14	Buksala	Porphyritic biotite monzonite granite	277.0 ± 2.4	Zircon LA-ICP-MS	4	Gao et al., 2010
15	Sorkuduk	Porphyritic biotite monzonite granite	280.9 ± 4.3	Zircon LA-ICP-MS	4	Gao et al., 2010
16	Qinghe	Blocket pegmatite	275.5 ± 4.2	Zircon LA-ICP-MS	3	Ren et al., 2011
17	Buerjing	Yelaman pegmatite	281 ± 10	Zircon SHRIMP	4	Sun et al., 2009b
18	Fuyun	Acidic dyke	286 ± 12	Zircon SIMS	5	Briggs et al., 2007
19	Fuyun	Acidic dyke	278 ± 7	Zircon SIMS	5	Briggs et al., 2007
20	Altai	Sarbulake	275.1 ± 1.7	Zircon SHRIMP	5	Sun, Long, et al., 2009
21	Mayinebo	S-type granite	283 ± 4	Zircon SHRIMP	Boundary of 4 and 5	Zhou et al., 2007
22	Fuyun	Diorite	277 ± 10	SIMS	5	Gong et al., 2007
23	Mayinebo	Granitic mylonite	281 ± 4	Zircon SHRIMP	5	Zhou et al., 2007
24	Dakeshiken	Alkali-rich granite	286 ± 1	TIMS	6	Tong et al., 2006
25	Altai	Lamazhao	276 ± 9	Zircon SHRIMP	4	Wang et al., 2005
26	Kalatongke	Norite	287 ± 5	Zircon SHRIMP	5	Han et al., 2004
27	Wuqiagou	Mafic intrusive	257.4 ± 5.3	Zircon SHRIMP	5	Chen & Han, 2006
28	FuyunWuqiagou	Basic granulite	268.0 ± 5.5	Zircon SHRIMP	4	Chen et al., 2006
29	FuyunWuqiagou	Basic granulite	271.0 ± 5.0	Zircon SHRIMP	4	Chen et al., 2006
30	FuyunWuqiagou	Basic granulite	271.0 ± 6.0	Zircon SHRIMP	4	Chen et al., 2006
31	FuyunWuqiagou	Basic granulite	279.0 ± 5.6	Zircon SHRIMP	4	Chen et al., 2006

Note. LA-ICP-MS = laser ablation inductively coupled plasma-mass spectrometry.

et al., 2012; Pankhurst, Vernon, Turner, Schaefer, & Foden, 2011; Trumbull, Harris, Frindt, & Wigand, 2004; Yang, Wu, Chung, Wilde, & Chu, 2006).

Extensive fractional crystallization of mantle-derived mafic magma is unlikely to produce Jiangjunshan and Dakalasu alkali-feldspar granites. First, large volumes of mafic-intermediate rocks, as would be expected if extensive fractional crystallization occurred, are absent in the study area. Second, the Jiangjunshan and Dakalasu alkali-feldspar granites possess some negative $\varepsilon_{Hf}(t)$ values, precluding the conclusion that the Jiangjunshan and Dakalasu alkali-feldspar granites were directly derived from the mantle source. On the basis of the geochemical and Sr-Nd-Hf isotopic data, Tong, Xu et al. (2014a) suggested that some Permian granitoids in the Chinese Altay were formed by fractionation of mantle-derived magmas contaminated by crustal material. As the Jiangjunshan and Dakalasu alkali-feldspar granites show much lower $\varepsilon_{Hf}(t)$ values than those of other granitoids (Figure 10), more crustal material was likely involved in the origin of the Jiangjunshan and Dakalasu alkali-feldspar granites. The zircon Hf isotope of the Jiangjunshan and Dakalasu alkali-feldspar granites is relatively uniform (with approximately 13 ε units, ranging from −7.0 to 5.6). Because the zircon Hf isotope does not change during partial melting or fractional crystallization, its heterogeneity most likely indicates that the Jiangjunshan and Dakalasu alkali-feldspar granites were derived from a mixed source, that is, partly juvenile and partly old crust (Yang et al., 2006).

The plot of La/Sm versus La shown in Figure 11a indicates a Rayleigh fractionation in a closed system during the evolutional process of the Jiangjunshan and Dakalasu alkali-feldspar granites. As shown in Figure 11b and 11c, fractional crystallization of plagioclase ± alkali-feldspar accounts for the change of Rb, Ba, and Sr with Eu. Depletion of Nb, Ta, Ti, and P in the Jiangjunshan and Dakalasu alkali-feldspar granites may indicate fractional crystallization of a titanium-rich mineral phase and apatite during magmatic evolution (Figure 11d).

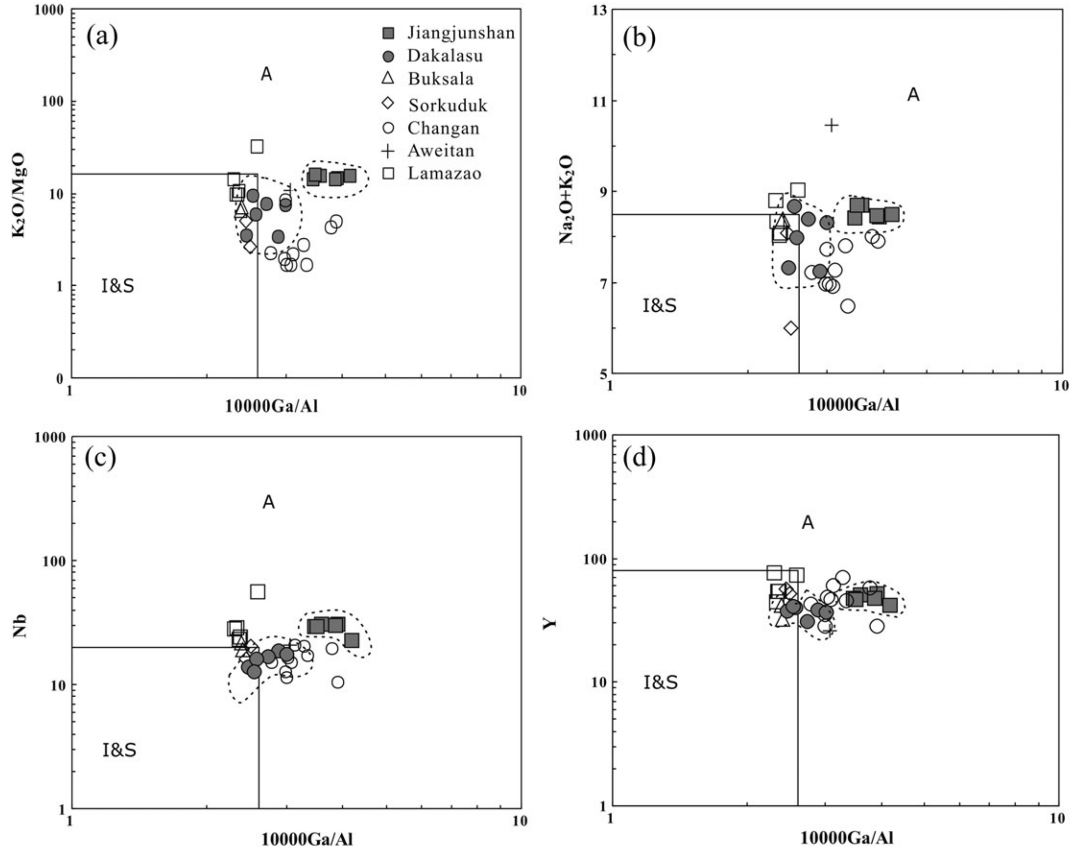

FIGURE 8 Chemical classification diagrams: (a) K_2O/MgO versus 10,000Ga/Al; (b) $K_2O + Na_2O$ versus 10,000Ga/Al; (c) Nb versus 10,000Ga/Al; and (d) Y versus 10,000Ga/Al

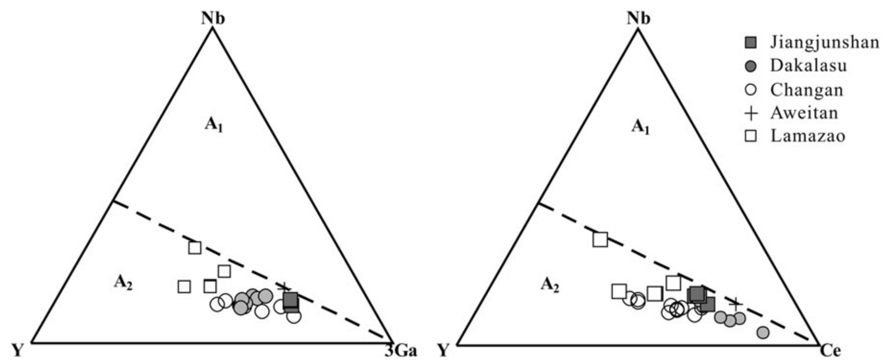

FIGURE 9 Y-Nb-Ga × 3 and Y-Nb-Ce diagrams of A-type granitoids from Jiangjunshan and Dakalasu (after Eby, 1992). A_1-anorogenic A-type granitoids and A_2-orogenic A-type granitoids

5.4 | Implications for tectonic evolution of the Chinese Altay

In this study, two Permian A-type granites are identified. In addition to the Jiangjunhshan and Dakalusu A-type granites, other coeval A-type granites are also identified in the Chinese Altay orogen with an intrusion age younger than 300 Ma, and these A-type granitic plutons are linearly distributed in the southern Chinese Altay (Figure 1). Several other tectonothermal events that are mainly bounded between the Abgong Fault and Erqis Fault and closely associated temporally with these A-type granites have also been reported. They include the following:

1. High-temperature (HT) and low-pressure metamorphism: A pelitic granulite has been confirmed with peak conditions of T = 780–800 °C and P = 5–6 kbar. SHRIMP zircon U–Pb dating presented a metamorphic age of 292.8 ± 2.3 Ma (Wang et al., 2009). The sillimanite-bearing metapelitic schist (635–670 °C and 5.8–6.8 kbar) was dated as 299.2 ± 3.4 Ma (Wang, Wei, Zhang, Chu, Zhao, & Liu, 2014b). Recently, two ~280-Ma pelitic granulites were identified, and the P–T estimates indicate peak conditions of >940 °C and 7.8–10 kbar and 970 °C and ~8 kbar, respectively (Li, Zhang, Chen, Zheng, Hollings, Wang, & Fang, 2014a; Tong, Xu et al., 2014a). These HT to ultrahigh-temperature and low-pressure metamorphic rocks reflect a high heat flow in the extensional environment in the Chinese Altay orogen during the Permian.
2. Mafic–ultramafic rock: Permian mafic–ultramafic intrusions or dykes are widely distributed only along the Irtish suture zone, and they comprise, from west to east, the Hongguleneng mafic–ultramafic complex (273.3 ± 2.6 Ma; Zhang et al., 2010), the Qiemuqieke hornblende-bearing gabbro (276.0 ± 2.1 Ma; Wan et al., 2013), the Kekesazi gabbro (281.2 ± 1.8 Ma) and mafic

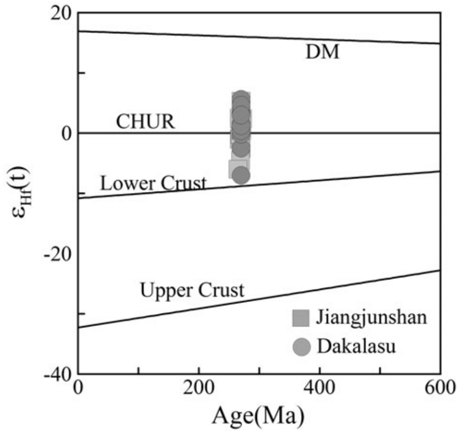

FIGURE 10 Hf isotopic diagram of the Jiangjunshan and Dakalasu pluton

dykes (279.6 ± 3.6 Ma; Zhang, Zou et al., 2014a), the Bayituobie gabbro (282.2 ± 2.8 Ma), the Jungeleke gabbro (283.6 ± 1.8 Ma), and the Palasier River gabbro (283.4 ± 1.4 Ma; Zhang, Zou et al., 2014a), the Kalatongke mafic–ultramafic complex (287 ± 5 Ma; Han et al., 2004), and the Mayinebo gabbro (272.5 ± 2.4 Ma) and the Dasazi gabbro (269.4 ± 2.5 Ma; Zhang et al., 2010). Geochemical data imply that these mafic–ultramafic rocks are predominantly derived from a subduction-metasomatized mantle wedge with variable degrees of crustal contamination. The gabbroic intrusions in the Dasazi region are part of a bimodal suite composed of A-type granitic plutons and high-Ti gabbroic intrusions (Zhang et al., 2010).

3. Felsic magmatism: In addition to A-type granites, some Permian I-type granites (~270 Ma) are identified. In general, these granites do not suffer from deformation and occur in a rounded shape in the southern Chinese Altay. Based on the geochemical data, these rocks are considered to be generated by differentiation of mantle-derived magmas with variable crustal contamination (Tong, Wang et al., 2014).
4. Regional uplift. The $^{40}Ar/^{39}Ar$ dating results of amphiboles from granite and amphibolites exposed in Alahake and Fuyun of the southern Chinese Altay yield consistent $^{40}Ar/^{39}Ar$ plateau ages of 265.9 ± 1.7 and 270.1 ± 3.1 Ma, which are younger than the ages of Permian HT metamorphism (~299–280 Ma; Li, Yuan, Sun, Long, & Cai, 2015). These ages may represent the timing of cooling of the amphiboles below the closure temperature after Early Permian HT metamorphism. The regional cooling is commonly associated with the uplift geological units in response to the crustal deformation (Reiners & Brandon, 2006; Stockli, 2005).

The geodynamic setting of the Chinese Altay in the Permian is debated, including the activity of mantle plumes (Tong, Xu et al., 2014a; Yang et al., 2015; Zhang, Zou et al., 2014a; Zhang et al.,

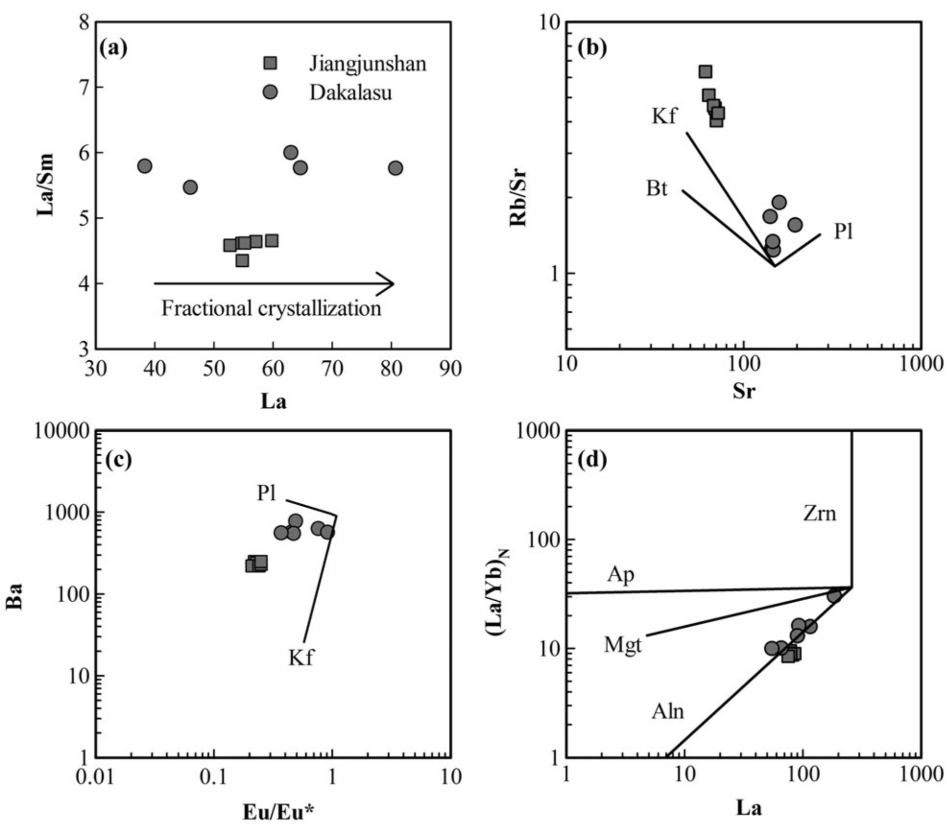

FIGURE 11 Trace-element diagrams for the evolution of the Jiangjunshan and Dakalasu granites: (a) La/Sm versus La; (b) Rb/Sr versus Sr, partition coefficients of Rb and Sr are from Philpotts and Schnetzler (1970); (c) Eu/Eu* versus Ba, partition coefficients are from Philpotts and Schnetzler (1970), Bacon and Druitt (1988), and Bea, Pereira, and Stroh (1994); (d) $(La/Yb)_N$ versus La, partition coefficients are from Fujimaki (1986) for apatite and Mahood and Hildreth (1983) for zircon, magnetite, and allanite. Pl = plagioclase; Kf = K-feldspar; AF = alkali feldspar Bt = biotite; Aln = allanite; Ap = apatite; Mgt = magnetite; Zrn = zircon

2012), slab break-off (Li, Yang et al., 2014b), postcollisional extension (Tong, Wang et al., 2014; Wang, Jahn, et al., 2014a; Wei et al., 2007), or a large-scale strike-slip shearing fault (Laurent-Charvet, Monié, Charvet, Shu, & Shi, 2003).

Mantle plume model: The coeval (275–270 Ma) voluminous, variably sourced mafic rocks in the Tarim and the mafic intrusions and voluminous A-type granites in Tianshan and Altay (see Zhang et al., 2010; Figure 1) constitute a Permian large igneous province in NW China. This large igneous province has been proposed to be the product of a ca. 280-Ma mantle plume (Qin et al., 2011; Su et al., 2011; Zhang et al., 2010). Nevertheless, we consider the mantle plume model implausible for a number of reasons. First, geochemical data confirm that the source of the Permian ultramafic–mafic rocks in the Chinese Altay orogen is strikingly different from those in the Tarim Craton. The former is derived from intensively depleted mantle and variably enriched by the Phanerozoic subduction slab-derived fluid or subducted sediments, whereas the latter is derived from enriched continental lithospheric mantle that has not been metasomatized by Phanerozoic subducted materials (Zhang et al., 2010). An HT mantle plume can melt down a refractory mantle beneath an old craton and give rise to a large igneous province, such as the Emeishan (Xu, He, Chung, Menzies, & Frey, 2004) and Siberian Traps (Sharma, 1997). If the mantle plume is emplaced beneath an orogenic belt in which the mantle has been water enriched, it will more easily melt to produce a larger volume of rock and then penetrate the lithospheric mantle, as in Yellowstone (Coble & Mahood, 2012). However, this is not the case in the southern Altaids, where the Permian mafic rocks are sporadically distributed linearly along the Erqis Fault and the amount of these Permian mafic rocks is considerably less than those of the previous Carboniferous arc rocks. Second, the A-type granites in the Chinese Altay are classified as A_2-type granites, which are significantly distinct from the Permian A_1-type granites in the Tarim craton, which are genetically related to the Tarim mantle plume.

Slab break-off model: Based on tectonothermal events, there is a general consensus that an extensional environment with high flow occurred in the southern margin of the Altay orogen during the Early Permian. The extensional environment can be related to the subduction, rift, and orogeny.

Because the known ophiolites in the Chinese Altay are older than the Early Permian and a late Carboniferous–Permian continental volcanic-sedimentary sequence abruptly overlapped the earlier Palaeozoic marine facies deposits in the southern Altay range, a collisional event in the Carboniferous is considered likely (Zhang, Zhao, et al., 2009a). Thus, the extensional environment caused by a back-arc or slab window associated with subduction has not been considered in this work.

The A_2-type granites are always associated with nonrift extensional environments (Eby, 1992). Recently, increasingly more Triassic rare element pegmatites have been reported in the Chinese Altay (Chen, 2011; Lv, Zhang, Tang, & Guan, 2012; Ma, 2014; Ren et al., 2011; Wang et al., 2007). According to the classification scheme presented by Cerny and Ercit (2005), these pegmatites belong to the Li, Cs and Ta (LCT) family, which may form in a postorogenic setting (Cerny, 1991). Thus, the extensional environment related to rift in the Permian, which usually is considered a tectonic setting for Nb, Y and F (NYF) pegmatites (Cerny, 1991), is ruled out.

Slab break-off usually occurs during the initial stages of continental collision, due to the contrasting strength and buoyancy between the subducting oceanic lithosphere and dragging continental lithosphere (Davies & von Blanckenburg, 1995). Slab break-off creates a combination of characteristic features of the orogenic belt, which is distinct from those suggested for other mechanisms, such as delamination. These features are as follows (Blanckenburg & Davies, 1995): (a) a narrow, linear zone of magmatism and metamorphism with a limited spatial distribution; (b) bimodal magmatism comprising basaltic partial mantle melts on the one hand and granitoids, most likely formed by lower crustal melting with a mantle parentage on the other hand; (c) regional HT metamorphism; (d) rapid uplifting and late exhumation; and (e) an extensional structure. These features are perfectly consistent with those tectonothermal events in the Chinese Altay in Permian. Therefore, we believe that slab break-off is the best model to account for the field observations and the characteristics of the magmatism and metamorphism in the Chinese Altay in the Permian.

The slab break-off model is also consistent with the tectonic history of the Chinese Altay. It has been shown that the 440- to 360-Ma granitic intrusions are widespread and represent the strongest episode of magmatic activity, Carboniferous intrusions (360–310 Ma) sporadically crop out in the southern Chinese Altay, Permian pluton (290–250 Ma) are widely distributed in the southern Chinese Altay and Erqis, and Triassic pegmatites mainly occur in the central Chinese Altay (Cai et al., 2011b and references therein; Zhang et al., 2016). These rocks correspond to the tectonic settings of subduction, transition from subduction to collision, the initial stages of continental collision, and postcollision. According to the 3-D numerical model proposed by van Hunen and Allen (2011), collision after the subduction leads to slab break-off at 20–25 Ma or 10 Ma later than the onset of continental collision, due to the different features of the subducting oceanic slab. If the ~300-Ma HT metamorphism represents the starting time of the slab break-off, it can be inferred that the collision between the Junggar and the Chinese Altay terranes most likely occurred at approximately 325 or 310 Ma.

6 | CONCLUSIONS

1. The zircon U–Pb dating indicates that the Jiangjunshan and Dakalasu granites were emplaced during the Middle Permian (268.3 ± 1.9 and 270.4 ± 1.9 Ma, respectively).
2. The Jiangjunshan and Dakalasu granites consist of A_2-type granite, based on their main and trace-element geochemical characteristics, indicating that the southern Altay was in a postcollision setting during the Late Permian.
3. The Jiangjunshan and Dakalasu granites show heterogeneous Hf isotope content, $\varepsilon_{Hf}(t)$ from −7.0 to +5.6, suggesting contributions from both the mantle and lower crust ends. Upwelling of the hot asthenospheric mantle after the collision and amalgamation between the Junggar and the Chinese Altay terranes most likely

triggered immediate mixing of mantle magma with the crust materials in the deep crust.

ACKNOWLEDGEMENTS

We thank the editors and the reviewers very much for their constructive comments that have greatly improved the manuscript. We thank Liu Xiaoming and Yuan Honglin for their help in determining the zircon Hf isotopic composition by LA-MC-ICP-MS. We also thank Li Liang for his assistance in zircon U–Pb dating by LA-ICP-MS. Many thanks to Ma Zhanlong for his assistance during the field work and sample analyses. This study was jointly supported by the Natural Science Foundation of China (Grant 41372104) and the National Supporting Program of China (305 Program; 2007BAB25B01).

REFERENCES

Anderson, I. C., Frost, C. D., & Frost, B. R. (2003). Petrogenesis of the Red Mountain pluton, Laramie anorthosite complex, Wyoming: Implications for the origin of A-type granite. *Precambrian Research*, *124*, 243–267. https://doi.org/10.1016/S0301-9268(03)00088-3

Bacon, C. R., & Druitt, T. H. (1988). Compositional evolution of the zoned calcalkaline magma chamber of Mount Mazama, Crater Lake, Oregon. *Contributions to Mineralogy and Petrology*, *98*, 224–256. https://doi.org/10.1007/BF00402114

Bea, F., Pereira, M. D., & Stroh, A. (1994). Mineral/leucosome trace-element partitioning in a peraluminous migmatite (a laser ablation-ICP-MS study). *Chemical Geology*, *117*, 291–312. https://doi.org/10.1016/0009-2541(94)90133-3

Blanckenburg, F., & Davies, J. H. (1995). Slab breakoff: A model for syncollisional magmatism and tectonics in the Alps. *Tectonics*, *14*, 120–131. https://doi.org/10.1029/94TC02051

Blichert-Toft, J., & Albarède, F. (1997). The Lu-Hf isotope geochemistry of chondrites and the evolution of the mantle–crust system. *Earth and Planetary Science Letters*, *148*(1), 243–258. https://doi.org/10.1016/S0012-821X(97)00040-X

Bonin, B. (2007). A-type granites and related rocks: Evolution of a concept, problems and prospects. *Lithos*, *97*, 1–29. https://doi.org/10.1016/j.lithos.2006.12.007

Briggs, S. M., Yin, A., Manning, C. E., Chen, Z. L., Wang, X. F., & Grove, M. (2007). Late Paleozoic tectonic history of the Ertix fault in the Chinese Altai and its implications for the development of the Central Asian orogenic system. *Geological Society of America Bulletin*, *119*, 944–960. https://doi.org/10.1130/b26044.1

Cai, K. D., Sun, M., Yuan, C., Long, X., & Xiao, W. (2011a). Geodynamics, tectonics, and metallogeny of orogenic belts, geological framework and Paleozoic tectonic history of the Chinese Altai, NW China: A review. *Russian Geology and Geophysics*, *52*, 1619–1633. https://doi.org/10.1016/j.rgg.2011.11.014

Cai, K. D., Sun, M., Yuan, C., Zhao, G., Xiao, W., Long, X., & Wu, F. (2011b). Geochronology, petrogenesis and tectonic significance of peraluminous granites from the Chinese Altai, NW China. *Lithos*, *127*, 261–281. https://doi.org/10.1016/j.lithos.2011.09.001

Cai, K. D., Sun, M., Xiao, W. J., Buslov, M. M., Yuan, C., Zhao, G. C., & Long, X. P. (2014). Zircon U–Pb geochronology and Hf isotopic composition of granitoids in Russian Altai Mountain, Central Asian Orogenic Belt. *American Journal of Science*, *314*, 580–612. https://doi.org/10.2475/02.2014.05

Cerny, P. (1991). Rare-element granite pegmatites part II. Regional to global environments and petrogenesis. *Geoscience Canada*, *18*, 68–81 .https://journals.lib.unb.ca/index.php/GC/article/view/3723/4237

Cerny, P., & Ercit, T. S. (2005). The classification of granitic pegmatites revisited. *Canadian Mineralogist*, *43*, 2005–2026. https://doi.org/10.2113/gscanmin.43.6.2005

Chen, J. F. (2011). Geochemistry of the plate part in Altai no.3 pegmatite and its formation and evolution. Master, Graduate University of Chinese Academy of Sciences, Beijing.

Chen, L. H., & Han, B. F. (2006). Geochronology, geochemistry and Sr-Nd-Pb isotopic composition of mafic intrusive rocks in Wuqiagou area, North Xinjiang: Constraints for mantle source and deep processes. *Acta Petrologica Sinica*, *22*, 1201–1214 (in Chinese with English Abstract).

Chen, B., & Jahn, B. M. (2002). Geochemical and isotopic studies of the sedimentary and granitic rocks of the Altai orogen of Northwest China and their tectonic implications. *Geological Magazine*, *139*, 1–13 .http://ci.nii.ac.jp/naid/80015400651/en/

Chen, H. L., Yang, S., Li, Z., Yu, X., Xiao, W., Yuan, C., … Li, J. (2006). Zircon SHRIMP U–Pb chronology of Fuyun basic granulite and its tectonic significance in Altaid orogenic belt. *Acta Petrologica Sinica*, *22*, 1351–1358 (in Chinese with English Abstract).

Chu, N. C., Taylor, R. N., Chavagnac, V., Nesbitt, R. W., Boella, R. M., Milton, J. A., … Burton, K. (2002). Hf isotope ratio analysis using multi-collector inductively coupled plasma mass spectrometry: An evaluation of isobaric interference corrections. *Journal of Analytical Atomic Spectrometry*, *17*, 1567–1574. https://doi.org/10.1039/b206707b

Clemens, J. D., Holloway, J. R., & White, A. J. R. (1986). Origin of an A-type granite: Experimental constraints. *American Mineralogist*, *71*, 317–324. https://www.mendeley.com/research/origin-atype-granite-experimental-constraints/

Cliff, R. A. (1985). Isotopic dating in metamorphic belts. *Journal of the Geological Society*, *142*, 97–110. https://doi.org/10.1144/gsjgs.142.1.0097

Coble, M. A., & Mahood, G. A. (2012). Initial impingement of the Yellowstone plume located by widespread silicic volcanism contemporaneous with Columbia River flood basalts. *Geology*, *40*, 655–658. https://doi.org/10.1130/g32692.1

Collins, W. J., Beams, S. D., White, A. J. R., & Chappell, B. W. (1982). Nature and origin of A-type granites with particular reference to southeastern Australia. *Contributions to Mineralogy and Petrology*, *80*, 189–200. https://doi.org/10.1007/bf00374895

Creaser, R. A., Price, R. C., & Wormald, R. J. (1991). A-type granites revisited: Assessment of a residual-source model. *Geology*, *19*, 163–166. https://doi.org/10.1130/0091-7613(1991)019<0163:atgrao>2.3.co;2

Dall'Agnol, R., & de Oliveira, D. C. (2007). Oxidized, magnetite-series, rapakivi-type granites of Carajás, Brazil: Implications for classification and petrogenesis of A-type granites. *Lithos*, *93*, 215–233. https://doi.org/10.1016/j.lithos.2006.03.065

Dall'Agnol, R., Scaillet, B., & Pichavant, M. (1999). An experimental study of a lower Proterozoic A-type granite from the Eastern Amazonian craton, Brazil. *Journal of Petrology*, *40*, 1673–1698. https://doi.org/10.1093/petroj/40.11.1673

Dallmeyer, R. D., & VanBreeman, O. (1981). Rb-Sr whole-rock and ^{40}Ar/^{39}Ar mineral ages of the Togus and Hallowell quartz monzonite and three mile pond granodiorite plutons, South-Central Maine: Their bearing on post-Acadian cooling history. *Contributions to Mineralogy and Petrology*, *78*, 61–73. https://doi.org/10.1007/bf00371144

Davies, J. H., & von Blanckenburg, F. (1995). Slab breakoff: A model of lithosphere detachment and its test in the magmatism and deformation of collisional orogens. *Earth and Planetary Science Letters*, *129*, 85–102. https://doi.org/10.1016/0012-821X(94)00237-S

Eby, G. N. (1990). The A-type granitoids: A review of their occurrence and chemical characteristics and speculations on their petrogenesis. *Lithos*, *26*, 115–134. https://doi.org/10.1016/0024-4937(90)90043-Z

Eby, G. N. (1992). Chemical subdivision of the A-type granitoids: Petrogenetic and tectonic implications. *Geology*, *20*, 641–644. https://doi.org/10.1130/0091-7613(1992)020<0641:csotat>2.3.co;2

Frost, C. D., & Frost, B. R. (1997). Reduced rapakivi-type granites: The tholeiite connection. *Geology*, *25*, 647–650. https://doi.org/10.1130/0091-7613(1997)025<0647:rrtgtt>2.3.co;2

Fujimaki, H. (1986). Partition-Coefficients of Hf, Zr, and Ree between Zircon, Apatite, and Liquid. *Contributions to Mineralogy and Petrology*, *94*(1), 42–45.

Gao, J. F., & Zhou, M. F. (2013). Magma mixing in the genesis of the Kalatongke dioritic intrusion: Implications for the tectonic switch from subduction to post-collision, Chinese Altay, NW China. *Lithos*, *162–163*, 236–250. https://doi.org/10.1016/j.lithos.2013.01.007

Gao, F. P., Zhou, G., Lei, Y. X., Wang, D. S., Chen, J. X., Zhang, H. F., … Zhao, H. H. (2010). Early Permian granite age and geochemical characteristics in Shaerbulake of Xinjiang's Altay area and its geological significance. *Geological Bulletin of China*, *29*, 1281–1293 (in Chinese with English abstract).

Gong, H. L., Chen, Z. L., Hu, Y. Q., Li, L., Lai, X. R., Ma, Q. Y., … Zhang, W. G. (2007). Geochemical characteristics of acidic dike swarm from the eastern segment of the Ertix tectonic belt, Altai orogeny and its geological implications. *Acta Petrologica Sinica*, *23*, 889–899. http://www.ysxb.ac.cn/ysxb/ch/reader/create_pdf.aspx?file_no=20070585andyear_id=2007andquarter_id=5andfalg=1

Griffin, W. L., Pearson, N. J., Belousova, E. A., & Saeed, A. (2006). Comment: Hf-isotope heterogeneity in zircon 91500. *Chemical Geology*, *23*, 358–363. https://doi.org/10.1016/j.chemgeo.2006.03.007

Griffin, W. L., Wang, X., Jackson, S. E., Pearson, N. J., O'Reilly, S. Y., Xu, X., & Zhou, X. (2002). Zircon chemistry and magma mixing, SE China: In-situ analysis of Hf isotopes, Tonglu and Pingtan igneous complexes. *Lithos*, *61*, 237–269. https://doi.org/10.1016/S0024-4937(02)00082-8

Han, B. F., Ji, J. Q., Song, B., Chen, L., & Li, Z. (2004). SHRIMP zircon U–Pb ages of Kalatongke no. 1 and Huangshandong Cu-Ni-bearing mafic-ultramafic complexes, North Xinjiang, and geological implications. *Chinese Science Bulletin*, *49*, 2424–2429 (in Chinese with English Abstract). https://doi.org/10.1007/bf03183432

Harrison, T. M., & McDougall, I. (1982). The thermal significance of potassium feldspar K-Ar ages inferred from $^{40}Ar^{39}Ar$ age spectrum results. *Geochimica et Cosmochimica Acta*, *46*, 1811–1820. https://doi.org/10.1016/0016-7037(82)90120-X

Hu, Z., Liu, Y., Chen, L., Zhou, L., Li, M., Zong, K., … Gao, S. (2011). Contrasting matrix induced elemental fractionation in NIST SRM and rock glasses during laser ablation ICP-MS analysis at high spatial resolution. [10.1039/C0JA00145G]. *Journal of Analytical Atomic Spectrometry*, *26*, 425–430. https://doi.org/10.1039/c0ja00145g

Jahn, B. M. (2004). The Central Asian Orogenic Belt and growth of the continental crust in the Phanerozoic. *Geological Society, London, Special Publications*, *226*, 73–100. https://doi.org/10.1144/gsl.sp.2004.226.01.05

Jahn, B. M., Wu, F. Y., & Chen, B. (2000a). Granitoids of the Central Asian Orogenic Belt and continental growth in the Phanerozoic. *Geological Society of America Special Papers*, *350*, 181–193. https://doi.org/10.1130/0-8137-2350-7.181

Jahn, B. M., Wu, F. Y., & Chen, B. (2000b). Massive granitoid generation in Central Asia: Nd isotope evidence and implication for continental growth in the Phanerozoic. *Episodes*, *23*, 82–92.

Jiang, N., Zhang, S., Zhou, W., & Liu, Y. (2009). Origin of a Mesozoic granite with A-type characteristics from the North China craton: Highly fractionated from I-type magmas? *Contributions to Mineralogy and Petrology*, *158*, 113–130. https://doi.org/10.1007/s00410-008-0373-2

Jung, S., Mezger, K., & Hoernes, S. (1998). Petrology and geochemistry of syn- to post-collisional metaluminous A-type granites—A major and trace element and Nd–Sr–Pb–O-isotope study from the Proterozoic Damara Belt, Namibia. *Lithos*, *45*, 147–175. https://doi.org/10.1016/S0024-4937(98)00030-9

Karsli, O., Caran, Ş., Dokuz, A., Çoban, H., Chen, B., & Kandemir, R. (2012). A-type granitoids from the Eastern Pontides, NE Turkey: Records for generation of hybrid A-type rocks in a subduction-related environment. *Tectonophysics*, *530–531*, 208–224. https://doi.org/10.1016/j.tecto.2011.12.030

Khain, E. V., Bibikova, E. V., Kröner, A., Zhuravlev, D. Z., Sklyarov, E. V., Fedotova, A. A., & Kravchenko-Berezhnoy, I. R. (2002). The most ancient ophiolite of the Central Asian fold belt: U–Pb and Pb–Pb zircon ages for the Dunzhugur complex, Eastern Sayan, Siberia, and geodynamic implications. *Earth and Planetary Science Letters*, *199*, 311–325. https://doi.org/10.1016/S0012-821X(02)00587-3

King, P. L., White, A. J. R., Chappell, B. W., & Allen, C. M. (1997). Characterization and origin of aluminous A-type granites from the Lachlan fold belt, southeastern Australia. *Journal of Petrology*, *38*, 371–391. https://doi.org/10.1093/petroj/38.3.371

Kinny, P. D., & Maas, R. (2003). Lu-Hf and Sm-Nd isotope systems in zircon. *Reviews in Mineralogy and Geochemistry*, *53*, 327–341. https://doi.org/10.2113/0530327

Knudsen, T.-L., Griffin, W., Hartz, E., Andresen, A., & Jackson, S. (2001). In-situ hafnium and lead isotope analyses of detrital zircons from the Devonian sedimentary basin of NE Greenland: A record of repeated crustal reworking. *Contributions to Mineralogy and Petrology*, *141*, 83–94. https://doi.org/10.1007/s004100000220

Kovalenko, V. I., Yarmolyuk, V. V., Kovach, V. P., Kotov, A. B., Kozakov, I. K., Salnikova, E. B., & Larin, A. M. (2004). Isotope provinces, mechanisms of generation and sources of the continental crust in the Central Asian mobile belt: Geological and isotopic evidence. *Journal of Asian Earth Sciences*, *23*, 605–627. https://doi.org/10.1016/S1367-9120(03)00130-5

Kröner, A., Demoux, A., Zack, T., Rojas-Agramonte, Y., Jian, P., Tomurhuu, D., & Barth, M. (2011). Zircon ages for a felsic volcanic rock and arc-related early Palaeozoic sediments on the margin of the Baydrag microcontinent, Central Asian Orogenic Belt, Mongolia. *Journal of Asian Earth Sciences*, *42*, 1008–1017. https://doi.org/10.1016/j.jseaes.2010.09.002

Kröner, A., Kovach, V., Belousova, E., Hegner, E., Armstrong, R., Dolgopolova, A., … Rytsk, E. (2014). Reassessment of continental growth during the accretionary history of the Central Asian Orogenic Belt. *Gondwana Research*, *25*, 103–125. https://doi.org/10.1016/j.gr.2012.12.023

Laurent-Charvet, S., Monié, P., Charvet, J., Shu, S. L., & Shi, M. R. (2003). Late-Paleozoic strike-slip shear zones in eastern Central Aisa (NW China): New structural and geochronological data. *Tectonics*, *22*, 1009–1032. https://doi.org/10.1029/2001TC901047

Li, X. R., Liu, F., & Yang, F. Q. (2012b). Geological times and its significance of the two mica syenogranite in the Keyinblack Cu-Zn deposit area in Altay, Xinjiang. *Xinjiang Geology*, *30*, 5–11 (in Chinese with English abstract).

Li, Z., Yang, X., Li, Y., Santosh, M., Chen, H., & Xiao, W. (2014b). Late Paleozoic tectono–metamorphic evolution of the Altai segment of the central Asian Orogenic Belt: Constraints from metamorphic P-T pseudosection and zircon U-Pb dating of ultra-high-temperature granulite. *Lithos*, *204*, 83–96. https://doi.org/10.1016/j.lithos.2014.05.022

Li, P., Yuan, C., Sun, M., Long, X., & Cai, K. (2015). Thermochronological constraints on the late Paleozoic tectonic evolution of the southern Chinese Altai. *Journal of Asian Earth Sciences*, *113*, 51–60. https://doi.org/10.1016/j.jseaes.2014.11.004

Li, D. F., Zhang, L., Chen, H. Y., Zheng, Y., Hollings, P., Wang, C. M., & Fang, J. (2014a). Ore genesis of the unusual Talate Pb-Zn(−Fe) skarn-type deposit, Altay, NW China: Constraints from geology, geochemistry and geochronology. *Geological Journal*, *49*, 599–616. https://doi.org/10.1002/gj.2570

Li, C., Zhang, M., Fu, P., Qian, Z., Hu, P., & Ripley, E. M. (2012a). The Kalatongke magmatic Ni–Cu deposits in the Central Asian Orogenic Belt, NW China: Product of slab window magmatism? *Mineralium Deposita*, *47*, 51–67. https://doi.org/10.1007/s00126-011-0354-7

Liu, Y., Gao, S., Hu, Z., Gao, C., Zong, K., & Wang, D. (2010b). Continental and oceanic crust recycling-induced melt–peridotite interactions in the trans-North China orogen: U–Pb dating, Hf isotopes and trace elements in zircons from mantle xenoliths. *Journal of Petrology*, *51*, 537–571. https://doi.org/10.1093/petrology/egp082

Liu, Y. S., Hu, Z. C., Zong, K. Q., Gao, C. G., Gao, S., Xu, J., & Chen, H. H. (2010a). Reappraisement and refinement of zircon U–Pb isotope and trace element analyses by LA-ICP-MS. *Chinese Science Bulletin*, *55*, 1535–1546 (in Chinese with English abstract).

Loiselle, M. C., & Wones, D. R. (1979). Characteristics and origin of anorogenic granites. *Geological Society of America Abstract with Programs*, *11*, 468.

Long, X., Sun, M., Yuan, C., Xiao, W., Lin, S., Wu, F., … Cai, K. (2007). U–Pb and Hf isotopic study of zircons from metasedimentary rocks in the

Chinese Altai: Implications for Early Paleozoic tectonic evolution. *Tectonics*, *26*(5), 1–20. https://doi.org/10.1029/2007TC002128

Long, X., Yuan, C., Sun, M., Xiao, W., Zhao, G., Wang, Y., … Xie, L. (2010). Detrital zircon ages and Hf isotopes of the early Paleozoic flysch sequence in the Chinese Altai, NW China: New constrains on depositional age, provenance and tectonic evolution. *Tectonophysics*, *480*, 213–231. https://doi.org/10.1016/j.tecto.2009.10.013

Lv, Z. H., Zhang, H., Tang, Y., & Guan, S. J. (2012). Petrogenesis and magmatic–hydrothermal evolution time limitation of Kelumute no. 112 pegmatite in Altay, northwestern China: Evidence from zircon UPb and Hf isotopes. *Lithos*, *154*, 374–391. https://doi.org/10.1016/j.lithos.2012.08.005

Ma, Z. L. (2014). Zircon U–Pb dating and Hf isotopes of Pegmatites from the Kaluan mining area in the Altay, Xinjiang and their genetic relationship with the Halong granite. In *The degree of master Of philosophy*. Beijing: Graduate University of Chinese Academy of Sciences.

Maniar, P. D., & Piccoli, P. M. (1989). Tectonic discrimination of granitoids. *Bulletin of the Geological Society of America*, *101*, 63–643. https://doi.org/10.1130/0016-7606(1989)101<0635:TDOG>2.3.CO;2

Mahood, G. A. & Hildreth, E. W. (1983). Large partition coefficients for trace elements in high-silica rhyolites. *Geochimica et Cosmochimica Acta*, *47*, 11–30. https://doi.org/10.1016/0016-7037(83)90087-X

Mansouri Esfahani, M., Khalili, M., Kochhar, N., & Gupta, L. N. (2010). A-type granite of the Hasan Robat area (NW of Isfahan, Iran) and its tectonic significance. *Journal of Asian Earth Sciences*, *37*, 207–218. https://doi.org/10.1016/j.jseaes.2009.05.010

Mezger, K. (1990). Geochronology in Granulites. In D. Vielzeuf, & P. Vidal (Eds.), *Granulites and crustal evolution*). Dordrecht: Springer Netherlands.

Mezger, K., Hanson, G. N., & Bohlen, S. R. (1989). High-precision U–Pb ages of metamorphic rutile: Application to the cooling history of high-grade terranes. *Earth and Planetary Science Letters*, *96*, 106–118. https://doi.org/10.1016/0012-821X(89)90126-X

Middlemost, E. A. K. (1994). Naming materials in the magma igneous rock system. *Earth-Science Reviews*, *37*, 215–224.

Namur, O., Charlier, B., Toplis, M. J., Higgins, M. D., Hounsell, V., Liégeois, J.-P., & Vander Auwera, J. (2011). Differentiation of Tholeiitic basalt to A-type granite in the Sept Iles layered intrusion, Canada. *Journal of Petrology*, *52*, 487–539. https://doi.org/10.1093/petrology/egq088

Pankhurst, M. J., Vernon, R. H., Turner, S. P., Schaefer, B. F., & Foden, J. D. (2011). Contrasting Sr and Nd isotopic behaviour during magma mingling; new insights from the Mannum A-type granite. *Lithos*, *126*, 135–146. https://doi.org/10.1016/j.lithos.2011.07.005

Patchett, P. J., Kouvo, O., Hedge, C. E., & Tatsumoto, M. (1981). Evolution of continental crust and mantle heterogeneity: evidence from Hf isotopes. *Contributions to Mineralogy and Petrology*, *78*, 279–297.

Philpotts, J. A., & Schnetzler, C. C. (1970). Phenocryst-matrix partition coefficients for K, Rb, Sr and Ba, with applications to anorthosite and basalt genesis. *Geochimica et Cosmochimica Acta*, *34*(3), 307–322. https://doi.org/10.1016/0016-7037(70)90108-0

Pirajno, F., Mao, J., Zhang, Z., Zhang, Z., & Chai, F. (2008). The association of mafic-ultramafic intrusions and A-type magmatism in the Tian Shan and Altay orogens, NW China: Implications for geodynamic evolution and potential for the discovery of new ore deposits. *Journal of Asian Earth Sciences*, *32*, 165–183. https://doi.org/10.1016/j.jseaes.2007.10.012

Qin, K. Z., Su, B. X., Sakyi, P. A., Tang, D. M., Li, X. H., Sun, H., … Liu, P. P. (2011). SIMS zircon U–Pb geochronology and Sr-Nd isotopes of Ni-Cu-bearing mafic-ultramafic intrusions in eastern Tianshan and Beishan in correlation with flood basalts in Tarim Basin (NW China): Constraints on a ca. 280 Ma mantle plume. *American Journal of Science*, *311*, 237–260. https://doi.org/10.2475/03.2011.03

Reiners, P. W., & Brandon, M. T. (2006). Using thermochronology to understand orogenic erosion. *Annual Review of Earth and Planetary Sciences*, *34*, 419–466. https://doi.org/10.1146/annurev.earth.34.031405.125202

Ren, B. Q., Zhang, H., Tang, Y., & Lv, Z. H. (2011). LA-ICPMS U–Pb zircon geochronology of the Altai pegmatites and its geological significance. *Acta Mineralogica Sinica*, *31*, 587–596 (in Chinese with English abstract).

Scherer, E., Munker, C., & Mezger, K. (2001). Calibration of the lutetium-hafnium clock. *Science (New York, N.Y.)*, *293*(5530), 683–687. https://doi.org/10.1126/science.1061372

Sengör, A. M. C., & Natal'in, B. A. (1996). Turkic-type orogeny and its role in the making of the continental crust. *Annual Review of Earth and Planetary Sciences*, *24*, 263–337. https://doi.org/10.1146/annurev.earth.24.1.263

Sengör, A. M. C., Natal'in, B. A., & Burtman, V. S. (1993). Evolution of the Altaid tectonic collage and Palaeozoic crustal growth in Eurasia. *Nature*, *364*(6435), 299–307. https://doi.org/10.1038/364299a0

Sharma, M. (1997). In J. J. Mahoney, & M. F. Coffin (Eds.), *Siberian traps. Large igneous provinces: Continental, oceanic, and planetary flood volcanism*). Washington DC: American Geophysical Union.

Shen, X., Zhang, H., Wang, Q., Wyman, D. A., & Yang, Y. (2011). Late Devonian–Early Permian A-type granites in the southern Altay range, Northwest China: Petrogenesis and implications for tectonic setting of “A$_2$-type” granites. *Journal of Asian Earth Sciences*, *42*, 986–1007. https://doi.org/10.1016/j.jseaes.2010.10.004

Stockli, D. F. (2005). Application of low-temperature thermochronometry to extensional tectonic settings. *Reviews in Mineralogy and Geochemistry*, *58*, 411–448. https://doi.org/10.2138/rmg.2005.58.16

Streckeisen, A. (1974). Classification and nomenclature of plutonic rocks. *Geologische Rundschau*, *63*, 773–786. https://doi.org/10.1007/BF01820841

Su, B. X., Qin, K. Z., Sakyi, P. A., Li, X. H., Yang, Y. H., Sun, H., … Malaviarachchi, S. P. K. (2011). U–Pb ages and Hf–O isotopes of zircons from Late Paleozoic mafic–ultramafic units in the southern Central Asian Orogenic Belt: Tectonic implications and evidence for an Early-Permian mantle plume. *Gondwana Research*, *20*, 516–531. https://doi.org/10.1016/j.gr.2010.11.015

Sun, G. H., Li, J. Y., Yang, T. N., Li, Y. P., Zhu, Z. X., & Yang, Z. Q. (2009a). Zircon SHRIMP U–Pb dating of two linear granite plutons in southern Altay Mountains and its tectonic implications. *Geology in China*, *36*(5), 976–987 (in Chinese with English abstract).

Sun, M., Long, X., Cai, K., Jiang, Y., Wang, B., Yuan, C., … Wu, F. (2009b). Early Paleozoic ridge subduction in the Chinese Altai: Insight from the abrupt change in zircon Hf isotopic compositions. *Science in China Series D: Earth Sciences*, *52*, 1345–1358. https://doi.org/10.1007/s11430-009-0110-3

Sun, M., Yuan, C., Xiao, W., Long, X., Xia, X., Zhao, G., … Kröner, A. (2008). Zircon U–Pb and Hf isotopic study of gneissic rocks from the Chinese Altai: Progressive accretionary history in the early to middle Palaeozoic. *Chemical Geology*, *247*, 352–383. https://doi.org/10.1016/j.chemgeo.2007.10.026

Sun, S. S., & McDonough, W. F. (1989). Chemical and isotopic systematics of oceanic basalt : implications for mantle composition and processes. *Geological Society London Special Publications*, *42*, 313–345. https://doi.org/10.1144/gsl.sp.1989.042.01.19

Tong, Y., Tao, W., Kovach, V. P., Hong, D.-w., & Han, B.-F. (2006). Age and origin of the Takeshiken postorogenic alkali-rich intrusive rocks in souther Altai, near the Mongolian border in China and its implications for continental growth. *Acta Petrologica Sinica*, *22*, 1267–1278 (in Chinese with English abstract).

Tong, Y., Wang, T., Jahn, B. M., Sun, M., Hong, D. W., & Gao, J. F. (2014b). Post-accretionary Permian granitoids in the Chinese Altai orogen: Geochronology, petrogenesis and tectonic implications. *American Journal of Science*, *314*, 80–109. https://doi.org/10.2475/01.2014.03

Tong, Y., Wang, T., Siebel, W., Hong, D.-W., & Sun, M. (2012). Recognition of Early Carboniferous alkaline granite in the southern Altai orogen: Post-orogenic processes constrained by U–Pb zircon ages, Nd isotopes, and geochemical data. *International Journal of Earth Sciences*, *101*, 937–950. https://doi.org/10.1007/s00531-011-0700-0

Tong, L. X., Xu, Y. G., Cawood, P. A., Zhou, X., Chen, Y., & Liu, Z. (2014a). Anticlockwise P–T evolution at ~280 Ma recorded from ultrahigh-temperature metapelitic granulite in the Chinese Altai Orogenic Belt, a possible link with the Tarim mantle plume? *Journal of Asian Earth Sciences*, *94*, 1–11. https://doi.org/10.1016/j.jseaes.2014.07.043

Trumbull, R. B., Harris, C., Frindt, S., & Wigand, M. (2004). Oxygen and neodymium isotope evidence for source diversity in Cretaceous anorogenic granites from Namibia and implications for A-type granite genesis. *Lithos*, *73*, 21–40. https://doi.org/10.1016/j.lithos.2003.10.006

van Hunen, J., & Allen, M. B. (2011). Continental collision and slab break-off: A comparison of 3-D numerical models with observations. *Earth and Planetary Science Letters*, *302*, 27–37. https://doi.org/10.1016/j.epsl.2010.11.035

Wan, B., Xiao, W., Windley, B. F., & Yuan, C. (2013). Permian hornblende gabbros in the Chinese Altai from a subduction-related hydrous parent magma, not from the Tarim mantle plume. *Lithosphere*, *5*, 290–299. https://doi.org/10.1130/l261.1

Wang, T., Hong, D. W., Jahn, B. M., Tong, Y., Wang, Y. B., Han, B. F., & Wang, X. X. (2006). Timing, petrogenesis, and setting of Paleozoic synorogenic intrusions from the Altai Mountains, Northwest China: Implications for the tectonic evolution of an accretionary orogen. *The Journal of Geology*, *114*, 735–751. https://doi.org/10.1086/507617

Wang, T., Hong, D. W., Yong, Y., Han, B. F., & Shi, Y. R. (2005). Zircon U–Pb SHRIMP age and origin of post-orogenic Lamazhao granite pluton from Altai orogen: Its implications for vertical continental growth. *Acta Petrologica Sinica*, *21*, 640–650 (in Chinese wtih English abstract).

Wang, T., Jahn, B. M., Kovach, V. P., Tong, Y., Wilde, S. A., Hong, D. W., … Salnikova, E. B. (2014a). Mesozoic intraplate granitic magmatism in the Altai accretionary orogen, NW China: Implications for the orogenic architecture and crustal growth. *American Journal of Science*, *314*, 1–42. https://doi.org/10.2475/01.2014.01

Wang, T., Tong, Y., Jahn, B. M., Zou, T. R., Wang, Y. B., Hong, D. W., & Han, B. F. (2007). SHRIMP U–Pb zircon geochronology of the Altai no. 3 pegmatite, NW China, and its implications for the origin and tectonic setting of the pegmatite. *Ore Geology Reviews*, *32*, 325–336. https://doi.org/10.1016/j.oregeorev.2006.10.001

Wang, W., Wei, C., Wang, T., Lou, Y., & Chu, H. (2009). Confirmation of pelitic granulite in the Altai orogen and its geological significance. *Chinese Science Bulletin*, *54*, 2543–2548. https://doi.org/10.1007/s11434-009-0041-6

Wang, W., Wei, C., Zhang, Y., Chu, H., Zhao, Y., & Liu, X. (2014b). Age and origin of sillimanite schist from the Chinese Altai metamorphic belt: Implications for Late Palaeozoic tectonic evolution of the Central Asian Orogenic Belt. *International Geology Review*, *56*, 224–236. https://doi.org/10.1080/00206814.2013.841335

Wang, Z. G., Zhao, Z. H., & Zou, T. R. (1998). *Geochemistry of the granitoids in Altay*. Beijing: Science Press.

Wei, C., Clarke, G., Tian, W., & Qiu, L. (2007). Transition of metamorphic series from the Kyanite-to andalusite-types in the Altai orogen, Xinjiang, China: Evidence from petrography and calculated KMnFMASH and KFMASH phase relations. *Lithos*, *96*, 353–374. https://doi.org/10.1016/j.lithos.2006.11.004

Whalen, J., Currie, K., & Chappell, B. (1987). A-type granites: Geochemical characteristics, discrimination and petrogenesis. *Contributions to Mineralogy and Petrology*, *95*, 407–419. https://doi.org/10.1007/bf00402202

Wilhem, C., Windley, B. F., & Stampfli, G. M. (2012). The Altaids of Central Asia: A tectonic and evolutionary innovative review. *Earth-Science Reviews*, *113*, 303–341. https://doi.org/10.1016/j.earscirev.2012.04.001

Windley, B. F., Alexeiev, D., Xiao, W., Kröner, A., & Badarch, G. (2007). Tectonic models for accretion of the Central Asian Orogenic Belt. *Journal of the Geological Society*, *164*, 31–47. https://doi.org/10.1144/0016-76492006-022

Windley, B. F., Kroner, A., Guo, J. H., Qu, G. S., Li, Y. Y., & Zhang, C. (2002). Neoproterozoic to Paleozoic geology of the Altai orogen, NW China: New zircon age data and tectonic evolution. *The Journal of Geology*, *110*, 719–737. https://doi.org/10.1086/342866

Wu, F. Y., Yang, Y. H., Xie, L. W., Yang, J. H., & Xu, P. (2006). Hf isotopic compositions of the standard zircons and baddeleyites used in U–Pb geochronology. *Chemical Geology*, *234*, 105–126. https://doi.org/10.1016/j.chemgeo.2006.05.003

Xiao, W., & Santosh, M. (2014). The western Central Asian Orogenic Belt: A window to accretionary orogenesis and continental growth. *Gondwana Research*, *25*, 1429–1444. https://doi.org/10.1016/j.gr.2014.01.008

Xiao, W. J., Han, C. M., Yuan, C., Sun, M., Lin, S., Chen, H., … Sun, S. (2008). Middle Cambrian to Permian subduction-related accretionary orogenesis of Northern Xinjiang, NW China: Implications for the tectonic evolution of Central Asia. *Journal of Asian Earth Sciences*, *32*, 102–117. https://doi.org/10.1016/j.jseaes.2007.10.008

Xiao, W., Windley, B. F., Badarch, G., Sun, S., Li, J., Qin, K., & Wang, Z. (2004). Palaeozoic accretionary and convergent tectonics of the southern Altaids: Implications for the growth of Central Asia. *Journal of the Geological Society*, *161*, 339–342. https://doi.org/10.1144/0016-764903-165

Xiao, W. J., Windley, B. F., Yuan, C., Sun, M., Han, C. M., Lin, S. F., … Sun, S. (2009). Paleozoic multiple subduction–accretion processes of the southern Altaids. *American Journal of Science*, *309*, 221–270. https://doi.org/10.2475/03.2009.02

Xiao, Y., Zhang, H., Shi, J. a., Su, B., Sakyi, P. A., Lu, X., … Zhang, Z. (2011). Late Paleozoic magmatic record of East Junggar, NW China and its significance: Implication from zircon U–Pb dating and Hf isotope. *Gondwana Research*, *20*, 532–542. https://doi.org/10.1016/j.gr.2010.12.008

Xu, J. F., Castillo, P. R., Chen, F. R., Niu, H. C., Yu, X. Y., & Zhen, Z. P. (2003). Geochemistry of late Paleozoic mafic igneous rocks from the Kuerti area, Xinjiang, Northwest China: Implications for backarc mantle evolution. *Chemical Geology*, *193*, 137–154. https://doi.org/10.1016/S0009-2541(02)00265-6

Xu, Y. G., He, B., Chung, S. L., Menzies, M. A., & Frey, F. A. (2004). Geologic, geochemical, and geophysical consequences of plume involvement in the Emeishan flood-basalt province. *Geology*, *32*, 917–920. https://doi.org/10.1130/g20602.1

Yang, T. N., Li, J. Y., Liang, M. J., & Wang, Y. (2015). Early Permian mantle–crust interaction in the south-central Altaids: High-temperature metamorphism, crustal partial melting, and mantle-derived magmatism. *Gondwana Research*, *28*, 371–390. https://doi.org/10.1016/j.gr.2014.05.003

Yang, J. H., Wu, F. Y., Chung, S. L., Wilde, S. A., & Chu, M. F. (2006). A hybrid origin for the Qianshan A-type granite, Northeast China: Geochemical and Sr–Nd–Hf isotopic evidence. *Lithos*, *89*, 89–106. https://doi.org/10.1016/j.lithos.2005.10.002

Yuan, C., Sun, M., Xiao, W., Li, X., Chen, H., Lin, S., … Long, X. (2007). Accretionary orogenesis of the Chinese Altai: Insights from Paleozoic granitoids. *Chemical Geology*, *242*, 22–39. https://doi.org/10.1016/j.chemgeo.2007.02.013

Zhang, S. H., Zhao, Y., Song, B., Hu, J. M., Liu, S. W., Yang, Y. H., … Liu, J. (2009a). Contrasting Late Carboniferous and Late Permian–Middle Triassic intrusive suites from the northern margin of the North China craton: Geochronology, petrogenesis, and tectonic implications. *Geological Society of America Bulletin*, *121*, 181–200. https://doi.org/10.1130/b26157.1

Zhang, Z. C., Zhou, G., Kusky, T. M., Yan, S., Chen, B., & Zhao, L. (2009b). Late Paleozoic volcanic record of the Eastern Junggar terrane, Xinjiang, Northwestern China: Major and trace element characteristics, Sr–Nd isotopic systematics and implications for tectonic evolution. *Gondwana Research*, *16*, 201–215. https://doi.org/10.1016/j.gr.2009.03.004

Zhang, L., Chen, H. Y., Zheng, Y., Qin, Y. J., & Li, D. F. (2014b). Geology, fluid inclusion and age constraints on the genesis of the Sarekuobu gold deposit in Altay, NW China. *Geological Journal*, *49*, 635–648. https://doi.org/10.1002/gj.2573

Zhang, Q. F., Hu, A. Q., Zhang, G. X., Fan, S. K., & Pu, Z. P. (1994). Evidence from isotopic age for presence of Mesozoic-Cenozoic magmatic activities in Altai region, Xinjiang. *Geochimica*, *23*, 269–280 (in Chinese with English abstract).

Zhang, C. L., Li, Z. X., Li, X. H., Xu, Y. G., Zhou, G., & Ye, H. M. (2010). A Permian large igneous province in Tarim and Central Asian Orogenic Belt, NW China: Results of a ca. 275 Ma mantle plume? *Geological Society of America Bulletin*, *122*, 2020–2040. https://doi.org/10.1130/b30007.1

Zhang, C. L., Santosh, M., Zou, H. B., Xu, Y. G., Zhou, G., Dong, Y. G., … Wang, H. Y. (2012). Revisiting the "Irtish tectonic belt": Implications for the Paleozoic tectonic evolution of the Altai orogen. *Journal of Asian Earth Sciences*, *52*, 117–133. https://doi.org/10.1016/j.jseaes.2012.02.016

Zhang, J., Sun, M., Schulmann, K., Zhao, G., Wu, Q., Jiang, Y., … Wang, Y. (2015). Distinct deformational history of two contrasting tectonic domains in the Chinese Altai: Their significance in understanding accretionary orogenic process. *Journal of Structural Geology*, *73*, 64–82. https://doi.org/10.1016/j.jsg.2015.02.007

Zhang, X., Zhang, H., Ma, Z. L., Tang, Y., Lv, Z. H., Zhao, J. Y., & Liu, Y. L. (2016). A new model for the granite-pegmatite genetic relationships in the Kaluan-Azubai-Qiongkuer pegmatite-related ore fields, the Chinese Altay. *Journal of Asian Earth Sciences*, *124*, 139–155. https://doi.org/10.1016/j.jseaes.2016.04.020

Zhang, C. L., Zou, H. B., Yao, C. Y., & Dong, Y. G. (2014a). Origin of Permian gabbroic intrusions in the southern margin of the Altai Orogenic Belt: A possible link to the Permian Tarim mantle plume? *Lithos*, *204*, 112–124. https://doi.org/10.1016/j.lithos.2014.05.019

Zheng, Y., Zhang, L., Chen, H., Li, D., Wang, C., & Fang, J. (2014). CO_2-rich fluid from metamorphic devolatilization of the Triassic orogeny: An example from the Qiaxia copper deposit in Altay, NW China. *Geological Journal*, *49*, 617–634. https://doi.org/10.1002/gj.2536

Zhou, G., Zhang, Z. C., Luo, S. B., He, B., Wang, X., Yin, L. J., … He, Y. K. (2007). Confirmation of high temperature strongly peraluminous Mayin'ebo granites in the south margin of Altay, Xinjiang: Age, geochemistry and tectonic implications. *Acta Petrologica Sinica*, *23*, 1909–1920 (in Chinese with English abstract).

SUPPORTING INFORMATION

Additional Supporting Information may be found online in the supporting information tab for this article.

How to cite this article: Liu Y, Zhang H, Tang Y, Zhang X, Lv Z, Zhao J. Petrogenesis and tectonic setting of the Middle Permian A-type granites in Altay, northwestern China: Evidences from geochronological, geochemical, and Hf isotopic studies. *Geological Journal*. 2018;53:527–546. https://doi.org/10.1002/gj.2910